Downloaded from rsta.royalsocietypublishing.org

PHILOSOPHICAL TRANSACTIONS OF THE ROYAL SOCIETY A MATHEMATICAL, PHYSICAL & ENGINEERING SCIENCES

The Deformation of Transversely Loaded Disks under Dynamic Loads

G. Munday and D. M. Newitt

Phil. Trans. R. Soc. Lond. A 1963 **256**, 1-30
doi: 10.1098/rsta.1963.0015

Email alerting service Receive free email alerts when new articles cite this article - sign up in the box at the top right-hand corner of the article or click **here**

To subscribe to *Phil. Trans. R. Soc. Lond. A* go to: **http://rsta.royalsocietypublishing.org/subscriptions**

This journal is © 1963 The Royal Society

Downloaded from rsta.royalsocietypublishing.org

THE DEFORMATION OF TRANSVERSELY LOADED DISKS UNDER DYNAMIC LOADS

By G. MUNDAY and D. M. NEWITT, F.R.S.
Department of Chemical Engineering and Chemical Technology, Imperial College, London, S.W.7

(*Received* 14 *November* 1962)

[Plates 1 and 2]

CONTENTS

	PAGE
1. Introduction	1
2. Equations of motion	2
2·1. Equations of motion of a wire	2
2·2. Equations of motion of a disk	5
3. The relations between deformation strain and stress	6
3·1. Strain displacement relations	6
3·2. Stress-strain relations	7
4. Solution of the equations of motion	8
4·1. The dynamic deflexion of a wire	8
4·2. The dynamic deflexion of a disk	14
5. Experimental	15
5·1. Equipment	15
(*a*) *The shock tube*	19
(*b*) *Deflexion measurement*	21
(*c*) *Disk material*	23
5·2. Performance of equipment	23
6. Results	25
7. Conclusions	28
References	29

The deformation of a thin flat metal disk under the influence of a transverse load is described, and the response times for the particular case of a copper disk have been determined experimentally. It is shown that the deflexion under shock loading conditions can be explained on the assumption that deformation is due to the combined action of inertia and strain waves. Comparison is made with the deflexion of an extensible wire under similar conditions and it is concluded that this simple analogy could be used as a basis for subsequent analysis.

1. Introduction

Thin metal disks are extensively used in the chemical industry to protect process vessels from sudden internal increases of pressure. These disks, called either bursting or rupture disks, are made of a ductile material and are clamped at the periphery over a venting area on the vessel. As the pressure behind the disk increases the material stretches and the disk bulges finally failing at the centre and opening up a vent for the release of pressure.

The plastic deformation of a disk under static loading conditions has been treated analytically by Swift (1952), Hill (1950) Brown & Thompson (1949), Gleyzal (1948), Brown & Sachs (1948), Kirkwood & Richardson (1944), and Weil & Newmark (1955). The last-named authors have given an analysis which appears to agree satisfactorily with experimental data for purely plastic deformation. However, the computations involve tedious trial-and-error integrations and Munday & Newitt (1962) have suggested a simplified approach.

Little information is available on the dynamic deformation of a disk, the most important paper being by Kirkwood & Richardson (1944). Their treatment, however, is of limited

The Royal Society is collaborating with JSTOR to digitize, preserve, and extend access to *Philosophical Transactions of the Royal Society of London. Series A, Mathematical and Physical Sciences.* www.jstor.org

Downloaded from rsta.royalsocietypublishing.org

use in determining the total time for deflexion of a real disk. The authors assume that the disk is made of a rigid plastic material and show that the plasticity equations predict constant stress throughout the disk, the stress being everywhere the yield stress. The resulting equation of motion is of the Lagrangian type and by a suitable Laplace transform can be solved for certain loading conditions.

Any extension of their analysis would require the introduction of strain hardening effects and the inclusion of stress wave propagation within the disk. The distribution of stresses and strains associated with strain hardening complicate the analysis and it is simpler to consider a one-dimensional system. The dynamic flexure of a wire is an example of a one-dimensional system comparable with the deflexion of a disk. It has been studied by Cristescu (1961) who showed that the deformation occurs through the interaction of two types of wave travelling along the wire.

In the present paper the equations for the deformation of both wire and disk for a constant load the direction of which is along the normal to the surface have been derived. A solution of the equations of motion is proposed for the wire for given boundary conditions and the deformation is described in terms of the propagation of two types of wave. It is also shown that this analysis, in which the two types of wave are considered separately, satisfies the general equations developed by Cristescu. In the case of the disk the equations cannot be solved without simplification and an assumption has been made to allow for comparison with the equations for the wire. This has suggested the possible extension of a similar numerical method to the solution of the three-dimensional system.

To test this hypothesis experimental evidence is required and equipment has been designed to measure the response time of a disk subjected to the sudden application of a transverse load produced at the end of an aerodynamic shock tube. The central deflexion of the disk is measured electronically and the variation in curvature photographically. The experimental results obtained in this way confirm the predicted mechanism of deformation and have been correlated for one disk material on the basis of its initial acceleration.

2. Equations of motion

The equations of motion of a deforming body are obtained by the application of the laws of conservation of momentum to an infinitesimal element. Such elements are shown in figures 1 and 2, the forces exerted on them by adjacent elements being designated R and the force exerted by the load normal to the element designated F. The resultant of these forces causes a change in momentum of the element in the direction A. If the variation of the forces R and the load from element to element at every instant of time is known the motion of the entire body can be computed.

The force vectors R are determined by the stress sustained by the element. Since the directions of these vectors are along the principal axes, their magnitudes are given by

$$R_i = (\text{stress in direction } i)\ (\text{thickness of element})\ (\text{width of element}).$$

2·1. *The equations of motion of a wire*

Before we set up the equations of motion and the boundary conditions, the problem must be defined more exactly. A convenient way of treating it is to consider a wire of square-section of thickness $\bar{h}$ and of initial length l freely supported at both ends in a magnetic field

Downloaded from rsta.royalsocietypublishing.org

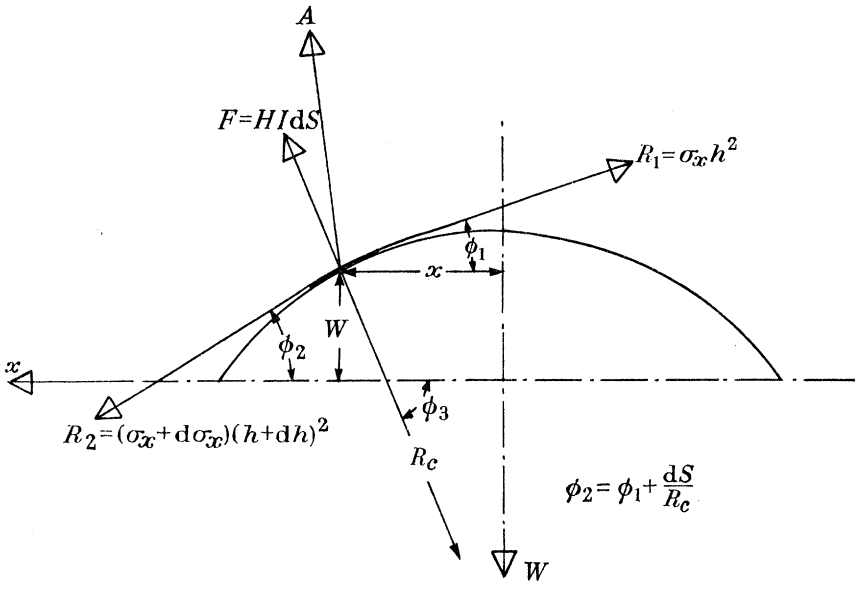

FIGURE 1. Forces acting on an element of wire. The direction of the W axis is reversed so that $\partial x/\partial S$ and R_c are positive.

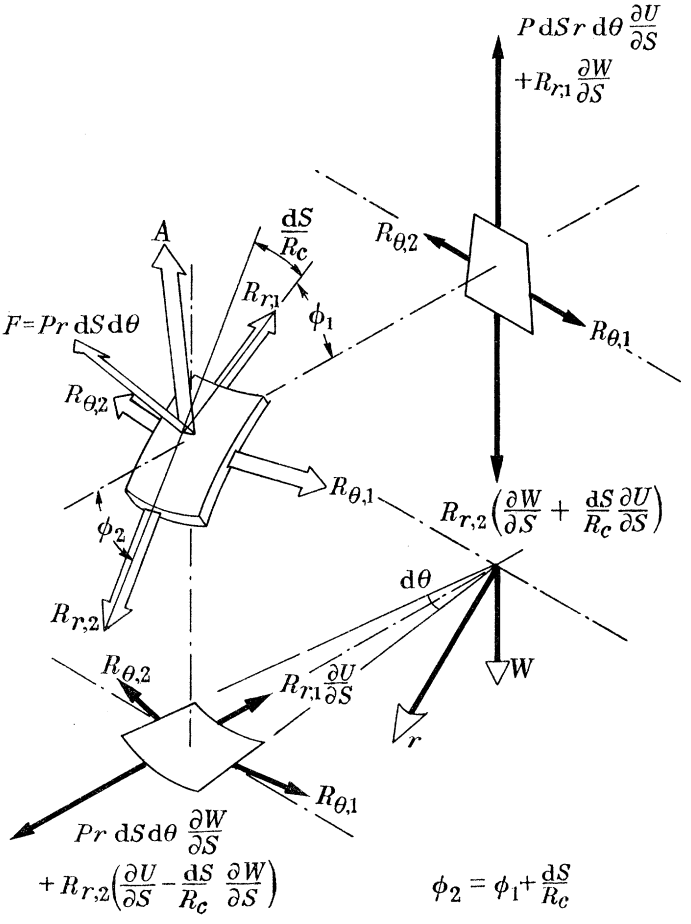

FIGURE 2. Forces acting on an element of the disk.

Downloaded from rsta.royalsocietypublishing.org

of field strength H. A current I, varying with time, passes through the wire and a force of magnitude HI per unit length is exerted on the wire. Assuming the bending moments are negligible and the wire undergoes plastic deformation only, it is necessary to determine the curvature of the wire and the stress distribution at all subsequent times.

The three vector forces are

$$R_1 = \sigma_x h^2,$$

$$R_2 = (\sigma_x + \mathrm{d}\sigma_x)\,(h+\mathrm{d}h)^2,$$

and

$$F = HI\,\mathrm{d}S,$$

with direction cosines referred to the horizontal axes of

$$\frac{\partial U}{\partial S}, \quad \frac{\partial U}{\partial S} - \frac{\mathrm{d}S}{R_c}\frac{\partial W}{\partial S} \quad \text{and} \quad \frac{\partial W}{\partial S},$$

respectively. The direction of the W axis is chosen so that the gradients and the radius of curvature are positive.

σ_x is the tensile stress in the element, x and W its position co-ordinates, $\mathrm{d}S$ its length and R_c its radius of curvature. U is the horizontal displacement of the element.

The two equations of motion are

$$h^2 G\rho \frac{\partial^2 U}{\partial t^2} = HI\frac{\partial W}{\partial x} + \frac{1}{G}\left(2h\sigma_x \frac{\partial h}{\partial x} + h^2 \frac{\partial \sigma_x}{\partial x}\right) - \sigma_x \frac{h^2}{R_c}\frac{\partial W}{\partial x} \tag{2·1}$$

in the horizontal direction and

$$-h^2 G\rho \frac{\partial^2 W}{\partial t^2} = HI - \frac{1}{G}\left(2h\sigma_x \frac{\partial h}{\partial x} + h^2 \frac{\partial \sigma_x}{\partial x}\right)\frac{\partial W}{\partial x} - \sigma_x \frac{h^2}{R_c} \tag{2·2}$$

in the vertical direction, where ρ is the density of the material and

$$G = \left[1 + \left(\frac{\partial W}{\partial x}\right)^2\right]^{\frac{1}{2}} = \frac{\partial S}{\partial x}. \tag{2·3}$$

The dimensionless terms

$$\left.\begin{aligned} \chi = \frac{x}{l}, \quad \omega = \frac{W}{l}, \quad \nu = \frac{U}{l}, \\ \xi = \frac{h}{\bar{h}}, \quad \tau = \left[\frac{m}{\rho l^2}\right]^{\frac{1}{2}} t \end{aligned}\right\} \tag{2·4}$$

are introduced, the overbar representing initial conditions, and equations (2·1) and (2·2) are simplified by substituting

$$R_c = \frac{[1 + (\partial W/\partial x)^2]^{\frac{3}{2}}}{\partial^2 W/\partial x^2} = \frac{G^3}{\partial^2 W/\partial x^2}$$

and

$$m = HI_0 l/h^2,$$

giving

$$G\frac{\partial^2 \nu}{\partial \tau^2} = \frac{1}{\xi^2}\frac{\partial \omega}{\partial \chi} + \frac{\sigma_x}{m}\frac{1}{G}\left(\frac{1}{\sigma_x}\frac{\partial \sigma_x}{\partial \chi} + \frac{2}{h}\frac{\partial h}{\partial \chi}\right) - \frac{\sigma_x}{m}\frac{1}{G^3}\frac{\partial^2 \omega}{\partial \chi^2}\frac{\partial \omega}{\partial \chi} \tag{2·5}$$

and

$$-G\frac{\partial^2 \omega}{\partial \tau^2} = \frac{1}{\xi^2} - \frac{\sigma_x}{m}\frac{1}{G}\left(\frac{1}{\sigma_x}\frac{\partial \sigma_x}{\partial \chi} + \frac{2}{h}\frac{\partial h}{\partial \chi}\right)\frac{\partial \omega}{\partial \chi} - \frac{\sigma_x}{m}\frac{1}{G^3}\frac{\partial^2 \omega}{\partial \chi^2}; \tag{2·6}$$

but

$$\frac{\sigma_x}{m}\frac{1}{G}\left(\frac{1}{\sigma_x}\frac{\partial \sigma_x}{\partial \chi} + \frac{2}{h}\frac{\partial h}{\partial \chi}\right) - \frac{\sigma_x}{m}\frac{1}{G^3}\frac{\partial^2 \omega}{\partial \chi^2}\frac{\partial \omega}{\partial \chi} = \frac{1}{\xi^2}\frac{\partial}{\partial \chi}\left(\frac{\sigma_x}{m}\frac{\xi^2}{G}\right)$$

Downloaded from rsta.royalsocietypublishing.org

and $$\frac{\sigma_x}{m}\frac{1}{G}\left(\frac{1}{\sigma_x}\frac{\partial\sigma_x}{\partial\chi}+\frac{2}{h}\frac{\partial h}{\partial\chi}\right)\frac{\partial\omega}{\partial\chi}+\frac{\sigma_x}{m}\frac{1}{G^3}\frac{\partial^2\omega}{\partial\chi^2}=\frac{1}{\xi^2}\frac{\partial}{\partial\chi}\left(\frac{\sigma_x}{m}\frac{\xi^2}{G}\frac{\partial\omega}{\partial\chi}\right);$$

therefore by combining these results with equations (2·3), (2·5) and (2·6) we have

$$\xi^2\frac{\partial^2 v}{\partial\tau^2}=\frac{\partial\omega}{\partial\psi}+\frac{\partial}{\partial\psi}\left(\frac{\sigma_x}{m}\xi^2\frac{\partial v}{\partial\psi}\right) \tag{2·7}$$

and $$-\xi^2\frac{\partial^2\omega}{\partial\tau^2}=\frac{\partial v}{\partial\psi}+\frac{\partial}{\partial\psi}\left(\frac{\sigma_x}{m}\xi^2\frac{\partial\omega}{\partial\psi}\right), \tag{2·8}$$

where $$\psi=S/l.$$

2·2. *The equations of motion of a disk*

A circular disk restrained at its rim in a horizontal plane and deformed by a transverse pressure has its principal axes of stress along the normal to the surface and in two directions tangential to the surface, one in the horizontal plane and the other in the vertical plane. An element, the boundaries of which are normal to these directions, is cut from the disk by two horizontal parallel planes and two vertical planes passing through the axis of the disk. The principal stresses are: σ_z the normal or thickness stress; σ_θ the circumferential or hoop stress; and σ_r the radial or transverse stress.

The forces in the principal directions are

$$R_{\theta,1}=R_{\theta 2}=\sigma_\theta h\,\mathrm{d}S,$$
$$R_{r,1}=\sigma_r hr\,\mathrm{d}\theta,$$
$$R_{r,2}=(\sigma_r+\mathrm{d}\sigma_r)\,(h+\mathrm{d}h)\,(r+\mathrm{d}r)\,\mathrm{d}\theta,$$

where h is the thickness of the element; $\mathrm{d}\theta$ the angle between the meridian planes; (W, r, θ) the position co-ordinates of the element; and $\mathrm{d}S$ its length in the vertical plane. The force exerted by the pressure P normal to the surface is

$$F=P\,\mathrm{d}S r\,\mathrm{d}\theta.$$

and the mass of the element is $$\rho h\,\mathrm{d}S r\,\mathrm{d}\theta.$$

By resolving the forces in horizontal and vertical directions as shown in figure 2, two equations of motion are obtained

$$hrG\rho\frac{\partial^2 U}{\partial t^2}=\frac{Pr\,\partial W}{\partial r}-\frac{\sigma_r}{R_c}hr\frac{\partial W}{\partial r}+\frac{1}{G}\left(h\sigma_r+hr\frac{\partial\sigma_r}{\partial r}+r\sigma_r\frac{\partial h}{\partial r}\right)-\sigma_\theta hG. \tag{2·9}$$

and $$-hrG\rho\frac{\partial^2 W}{\partial t^2}=Pr-\frac{\sigma_r}{R_c}hr-\frac{1}{G}\frac{\partial W}{\partial r}\left(h\sigma_r+hr\frac{\partial\sigma_r}{\partial r}+r\sigma_r\frac{\partial h}{\partial r}\right), \tag{2·10}$$

where W and U are the vertical and horizontal displacements of the element,

$$G=\left[1+\left(\frac{\partial W}{\partial r}\right)^2\right]^{\frac{1}{2}}=\frac{\partial S}{\partial r}$$

and R_c is the radius of curvature of the element in the vertical plane. A third equation, obtained by resolving in the third direction, is redundant for reasons of symmetry.

Downloaded from rsta.royalsocietypublishing.org

The dimensionless groups are

$$\left.\begin{aligned} \eta &= \frac{r}{R}, \quad \omega = \frac{W}{R}, \quad \nu = \frac{U}{R}, \\ \xi &= \frac{h}{\bar{h}}, \quad \tau = \left[\frac{P_0}{R\bar{h}\rho}\right]^{\frac{1}{2}} t. \end{aligned}\right\} \tag{2·11}$$

P_0 is a constant to be defined later and the pressure term is rewritten $p = PR/\bar{h}$. R without a subscript, is the radius of the disk.

The equations are rearranged in a manner similar to that for the wire, to give

$$\xi\eta \frac{\partial^2 \nu}{\partial \tau^2} = \frac{p}{p_0}\eta \frac{\partial \omega}{\partial \psi} + \frac{\partial}{\partial \psi}\left(\xi\eta \frac{\sigma_r}{p_0}\frac{\partial \nu}{\partial \psi}\right) - \frac{\sigma_\theta}{p_0}\xi \tag{2·12}$$

and

$$-\xi\eta \frac{\partial^2 \omega}{\partial \tau^2} = \frac{p}{p_0}\eta \frac{\partial \nu}{\partial \psi} - \frac{\partial}{\partial \psi}\left(\xi\eta \frac{\sigma_r}{p_0}\frac{\partial \omega}{\partial \psi}\right), \tag{2·13}$$

where

$$\psi = S/R.$$

3. The relations between deformation, strain and stress

The solution of the equations of motion requires a knowledge of the stress and strain distribution throughout the body. The strain is fixed by the degree of deformation of the elements and is expressed in terms of the stress in the element by relations which idealize the behaviour of the material. These equations can be developed in mathematical terms (Munday 1961).

3·1. *The strain displacement relations*

The relation between the deformation of a system and the strain in an element of it is established by examining its history during displacement. The strain is defined by the change in length of the element and, for large strain met with in plastic deformation, the natural strain in the ith direction is defined by

$$\epsilon_i = \ln (\partial S/\partial \bar{S})_i. \tag{3·1}$$

That is, the strain-displacement relation is obtained from the ratio of the instantaneous to the initial length of a line element.

For the wire

$$\epsilon_x = \ln\left\{\frac{[1+(\partial\omega/\partial\chi)^2]^{\frac{1}{2}}}{1-(\partial\nu/\partial\chi)}\right\} \tag{3·2}$$

and

$$\epsilon_y = \epsilon_z = \ln (h/\bar{h}). \tag{3·3}$$

For the disk

$$\epsilon_\theta = \ln\{\eta/(\eta-\nu)\}, \tag{3·4}$$

$$\epsilon_r = \ln\left\{\frac{[1+(\partial\omega/\partial\eta)^2]^{\frac{1}{2}}}{1-(\partial\nu/\partial\eta)}\right\}, \tag{3·5}$$

$$\epsilon_z = \ln (h/\bar{h}), \tag{3·6}$$

where ϵ_θ, ϵ_r and ϵ_z are the circumferential, radial and normal strains, respectively (Munday & Newitt 1962).

Downloaded from rsta.royalsocietypublishing.org

3·2. *Stress-strain relations*

The stress-strain relations for plastic deformation are expressed as two sets of equations. The first, the equations of plasticity, relates components of stress to components of strain in the principal directions. The two main theories, the Saint-Venant theory of plastic deformation and Hencky's plastic flow theory, postulate proportionality between components of stress deviation and corresponding components of strain deviation. The proportionality factor will vary from element to element, since the stress and strain must also obey the 'universal' stress-strain relation. This forms the second set of equations and depends on the material only, being independent of the configuration of the applied forces and the shape of the body under strain.

The equations of plasticity used in this paper are

$$\left.\begin{aligned} 2\sigma_1-\sigma_2-\sigma_3 &= 6G_p\epsilon_1,\\ 2\sigma_2-\sigma_3-\sigma_1 &= 6G_p\epsilon_2,\\ 2\sigma_3-\sigma_1-\sigma_2 &= 6G_p\epsilon_3,\end{aligned}\right\} \tag{3·7}$$

where

$$G_p = f(\sigma_d, \epsilon_d)$$

and subscripts 1, 2 and 3 refer to the principal directions. σ_d and ϵ_d are the largest principal or 'decisive', stress and strain, respectively, and it is assumed that the former is a unique function of the latter. This statement takes the place of the considerably more complicated 'universal' stress-strain relations based on the yield criteria of von Mises and Tresca. Equations (3·7) include, implicitly, the incompressibility equation

$$\epsilon_1+\epsilon_2+\epsilon_3 = 0. \tag{3·8}$$

For the wire, the plasticity equations simplify to the condition of incompressibility and, since the strains in the directions perpendicular to the axis of the wire are equal,

$$\epsilon_y = \epsilon_z = -\tfrac{1}{2}\epsilon_x \tag{3·9}$$

The decisive strain is therefore ϵ_x and, since the stresses in the y and z directions can be assumed negligible, the universal stress-strain relation is

$$\sigma_x = f(|\epsilon_x|). \tag{3·10}$$

It should be noted here that tensile stresses and strains are positive.

The normal stress in the disk is assumed to be zero and the plasticity equations can be written

$$\frac{2(\sigma_r/\sigma_\theta)-1}{(\sigma_r/\sigma_\theta)+1} = -\frac{\epsilon_r}{\epsilon_z} \tag{3·11}$$

and

$$\epsilon_r+\epsilon_\theta+\epsilon_z = 0. \tag{3·12}$$

The third equation involves the function relating G_p to the principal stresses and strains by the universal stress-strain relation. This function is normally expressed in terms of the octahedral shear stress and strain but a reasonable approximation is obtained by

$$G_p = \tfrac{1}{3}(\sigma_d/\epsilon_d)$$

when the decisive stresses and strains are used.

At the rim of the disk the circumferential strain is zero and equations (3·11) and (3·12) yield $\sigma_r = 2\sigma_\theta$. At the centre the circumferential and radial stresses are identical and hence

Downloaded from rsta.royalsocietypublishing.org

it can be assumed that $\sigma_r > \sigma_\theta$ in most cases and the decisive stress is that in the radial direction. Similarly it can be shown that the largest strain occurs in the normal direction.

Therefore

$$\left.\begin{aligned} \sigma_d &= \sigma_r \\ \text{and} \quad \epsilon_d &= |\epsilon_z|. \end{aligned}\right\} \tag{3·13}$$

It should be remembered that the normal strain is compressive and negative and the decisive strain only refers to its numerical value.

4. Solution of the equations of motion

The equations of motion, can be related to the physical process of deformation by examining each term.

(i) The left-hand side of the equation represents the acceleration of an element of unit length $d\psi$, in which the variation in thickness ratio ξ (and in the case of the disk, its position) is taken into account.

(ii) The first term on the right-hand side of the equation represents the forces exerted by adjacent elements. These are independent of thickness but depend upon the size of the element (and hence, in the case of the disk, upon its position).

(iii) The second term on the right-hand side represents the resultant force due to the change in stress across the element depending on the change in stress, element thickness and size.

(iv) The last term, in equation (2·12) for the disk, represents the force exerted by adjacent elements in the circumferential direction which depends upon the element thickness and the circumferential stress.

Equations (2·7) and (2·8) for the wire are hyperbolic differential equations which can be solved by the application of the method of characteristics. A purely analytical solution is not possible and certain simplifying assumptions have been made. These have resulted in a clearer picture of the mode of deformation and it has been possible to assess the effects of the factors neglected in the assumptions.

The equations of motion for the disk are similar in form to those for the wire, but the term involving the circumferential stress precludes any characteristic solution. Here again simplifying assumptions are made which suggest, by analogy with the wire, a possible analytical approach.

4·1. *The dynamic deflexion of a wire*

If the wire is made from a perfectly plastic material, so that σ_x is constant, and if the change in thickness is neglected, the two equations of motion can be simplified to give

$$\frac{\partial^2 v}{\partial \tau^2} = \frac{\partial \omega}{\partial \psi} + \frac{\sigma_x}{m}\frac{\partial^2 v}{\partial \psi^2}$$

and

$$-\frac{\partial^2 \omega}{\partial \tau^2} = \frac{\partial v}{\partial \psi} - \frac{\sigma_x}{m}\frac{\partial^2 \omega}{\partial \psi^2}.$$

These can be solved graphically by the use of a single net of characteristic lines. However, a clearer physical picture is obtained, particularly of the later stages of deformation, if only the second of these equations is used and the horizontal acceleration is neglected, i.e.

$$-\frac{\partial^2 \omega}{\partial \tau^2} = 1 - \frac{\sigma_x}{m}\frac{\partial^2 \omega}{\partial \psi^2} \tag{4·1}$$

PHILOSOPHICAL TRANSACTIONS OF THE ROYAL SOCIETY A MATHEMATICAL, PHYSICAL & ENGINEERING SCIENCES

PHILOSOPHICAL TRANSACTIONS OF THE ROYAL SOCIETY A MATHEMATICAL, PHYSICAL & ENGINEERING SCIENCES

Downloaded from rsta.royalsocietypublishing.org

if $\partial\omega/\partial\psi$ is small. The initial conditions are at

$$\tau = 0; \quad \omega = 0, \quad \partial\omega/\partial\tau = 0 \quad \text{and} \quad I = 0$$

and for a wire suddenly loaded with a current pulse of constant magnitude I_0 the boundary conditions are for all $\tau \geqslant 0$; $I = I_0$ and $\omega = 0$ at $\chi = 1$. This second-order partial differential equation has the solution:

$$-\omega = \tfrac{1}{2}\tau^2 \quad \text{when} \quad (1-\psi) \geqslant a\tau, \tag{4·2a}$$

$$-\omega = \tfrac{1}{2}a^2[2a(1-\psi)\,\tau - (1-\psi)^2] \quad \text{when} \quad (1-\psi) \leqslant a\tau, \tag{4·2b}$$

where

$$a^2 = \sigma_x/m.$$

Equation (4·2a) describes the motion of a free wire; hence the central section of the wire moves initially as a free body and is flat; subsequently the flatness is destroyed by a transverse wave, represented by equation (4·2b), travelling from the ends with a velocity a. The dimensionless velocity of a particle in the central section has the value τ and has a constant dimensionless acceleration of unity. All other particles have a velocity

$$-\partial\omega/\partial\tau = (1-\psi)/a \tag{4·3}$$

and zero acceleration. Thus as the wave passes the particle its acceleration is reduced immediately from unity to zero. When the wave reaches the centre of the wire the velocity of all the particles is given by equation (4·3) and the acceleration is everywhere zero.

The next phase of the motion involves the deceleration of the wire until it comes to rest. The equation of motion (4·1), is still valid but new boundary conditions imply that a 'retarding wave' travels back along the wire bringing each element, in turn, to rest with respect to its neighbour, so that when this wave reaches the fixed ends of the wire the velocity of all the elements is zero. This assumes that no further wave reflexions occur. Since experimental evidence shows that the later reflexions that do occur are of small amplitude this is a reasonable approximation. However, a rigid analysis would have to take into account the nature of the interaction of the two waves travelling in opposite directions; the velocity of the wire when the resultant wave reaches the ends may not be zero.

The analysis of this second phase yields the solution

$$-\omega = [2a\tau(1-\psi) - (1-\psi)^2]/2a^2, \quad \text{when} \quad (1-\psi) \leqslant (2-a\tau) \tag{4·4}$$

(elements not yet influenced by the second wave),

$$-\omega = [a\tau(4-a\tau) - 2(\psi^2+1)]/2a^2, \quad \text{when} \quad (1-\psi) \geqslant (2-a\tau) \tag{4·5}$$

(elements that have been affected by both incident and reflected wave).

Before a particle is subject to the retarding wave it has a velocity given by

$$-\partial\omega/\partial\tau = (1-\psi)/a \tag{4·6}$$

and is independent of τ. Its acceleration is zero. After the wave has passed the particle its velocity becomes

$$-\partial\omega/\partial\tau = (2-a\tau)/a \tag{4·7}$$

and is independent of ψ. Its deceleration is then unity.

These results, translated into terms of S, σ_x, h, W, t show that, when the wire is subjected to a suddenly applied transverse load, it deforms under the action of a wave travelling

Downloaded from rsta.royalsocietypublishing.org

through the wire at a speed proportional to the inverse root of the material density. The wave starts at the fixed ends and is reflected at the centre, the wire being brought to rest when the wave reaches the ends again. The centre of the wire is accelerated at a constant rate dependent on the loading, the thickness of the wire and its density and then decelerated for an equal period of time at the same rate until it comes to rest. The maximum velocity occurs half way through the deformation and its magnitude is proportional to the loading and inversely proportional to the square root of the density. It is also directly proportional to the length of the wire and inversely proportional to the square root of its thickness.

The positions of the wire in the two phases of deformation are shown in figure 3. In the first phase the variation of stress and the change in curvature are small so that this approximate solution is reasonably accurate. During the second phase these deviations are much greater and the discrepancies in equation (4·1) are of the order of 50 %.

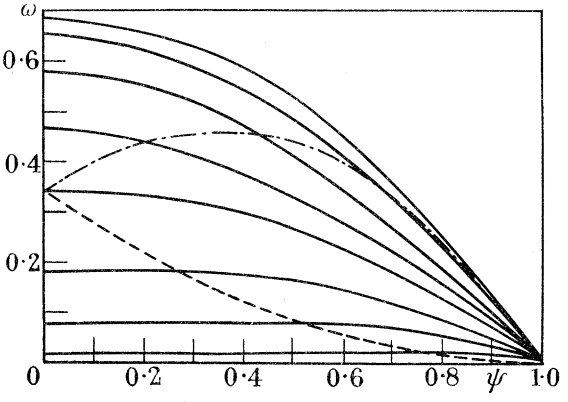

FIGURE 3. Dynamic deflexion of a wire. ———, The position of the wire after intervals of $\tau = 0{\cdot}2$, – – – –, incident inertia wave; —·—·—, reflected inertia wave.

This simple analysis neglects the effect of strain hardening and it will now be necessary to consider how the increase in stress, due to this hardening, affects the subsequent motion. The deformation of the wire by the inertia wave strains the material, and, since the wire is held at the ends only strain initially occurs at these points. Strain requires the movement of material and will therefore need a finite time to travel through the wire. The velocity of this strain disturbance has been determined both experimentally and analytically by a number of workers (Kolsky 1953; Craggs 1961). The velocity of the strain wave is dependent upon the magnitude of the strain and, for most materials, large strains are propagated with velocities lower than those for small strains.

For a wire under uniaxial dynamic load the strain is distributed by waves whose velocities, C, depend upon the magnitude of the stress-strain gradient and

$$C = \left[\frac{1}{\rho}\frac{\partial \sigma_x}{\partial \epsilon_x}\right]^{\frac{1}{2}}, \tag{4·8}$$

where $\partial \sigma_x / \partial \epsilon_x$, the tangent modulus of the material, is dependent upon the strain.

As the wire is strained by the passage of the inertia wave, the strain at the ends increases and a succession of strain disturbances are generated. These travel through the wire at decreasing velocities. At some stage the increase in length produced by the expanding fan

Downloaded from rsta.royalsocietypublishing.org

of strain disturbances is sufficient to allow the inertia wave to propagate without further straining at the ends. No further disturbances are produced and a discrete wave will proceed down the wire, the stress at the head of the wave being at the yield value (zero plastic strain) and that at the tail having a value corresponding to the strain induced at the

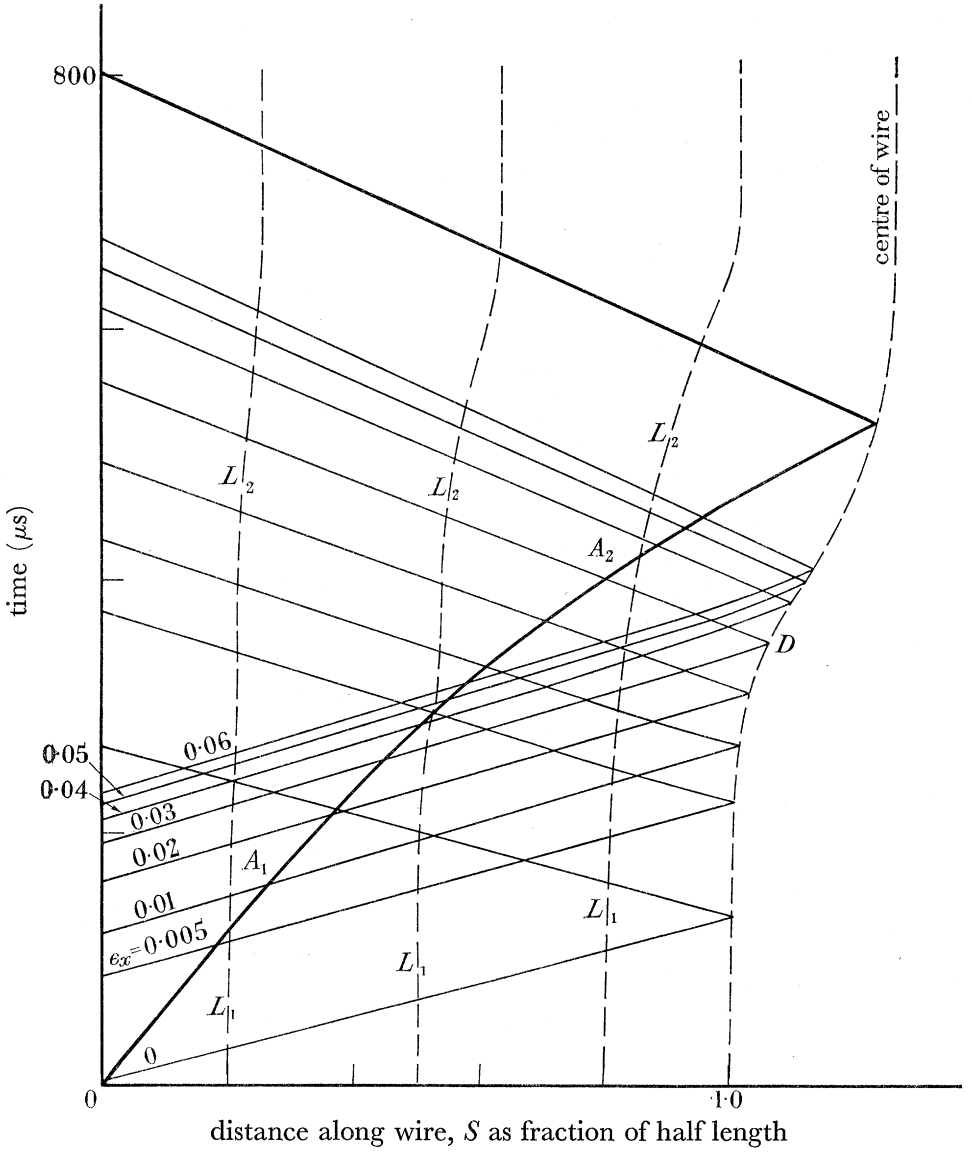

FIGURE 4. Wave diagram. Diagrammatic representation of wave interactions in a 4 in. long copper wire.

ends by the inertia wave. If the restraint at the ends of the wire falls, the stress within the plastic wave is reduced by the transmission of elastic unloading waves as described by Goldsmith (1960). When the elastic unloading wave overtakes the plastic wave, it reduces the intensity of the stress in the wave and is reflected back towards the ends. The repeated reflexion of elastic waves between the ends of the wire and the plastic wave reduces the stress until the forces at the ends of the wire are compatible with the strain requirements of the inertia wave.

Downloaded from rsta.royalsocietypublishing.org

The effect of the combination of inertia and plastic waves is best explained on a wave diagram. One of the difficulties in describing the deformation of the wire on the wave diagram is that a three-dimensional picture is required, one dimension representing time and the other two the spatial position of the wire. This is overcome by using the wave diagram illustrated in figure 4 in which the wave motion is considered to take place along the wire and the axes are chosen so that the abscissa represents the distance S along the wire and the ordinate the time t.

The full thick line is the trajectory of the discontinuity (or inertia wave) and the groups of fine lines represent the plastic wave. The movement of elements in the wire are indicated by dashed lines. This diagram has been drawn on the basis of the stress-strain curve for

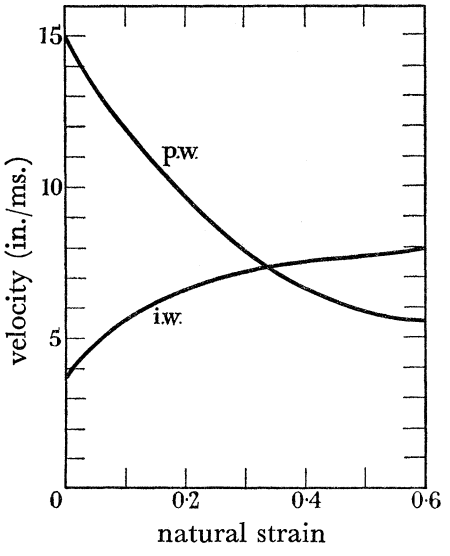

FIGURE 5. Wave velocities in copper wires: p.w., plastic wave; i.w., inertia wave. Velocity of elastic wave = 1445 in./ms.

copper assuming that it is not affected by rate of strain. The velocities of inertia, plastic-strain and elastic-strain waves calculated from the stress-strain diagram for copper given by Mellor (1956) are shown in figure 5.

The velocity V of an element of the wire is given by the integrated effect of the strains between the element and the end of the wire.

$$V = \int_0^{\epsilon_x} \left(\frac{1}{\rho}\frac{\partial \sigma_x}{\partial \epsilon_x}\right)^{\frac{1}{2}} \mathrm{d}\epsilon_x. \tag{4·9}$$

The velocity of a strain wave through space is the sum of this velocity and the strain velocity, C, namely $V+C$. Thus both the paths of the elements and the points of constant strain can be calculated.

The inertia wave causing the straining travels at a velocity given by

$$a_0 = \sqrt{(\sigma_x/\rho)}$$

and for most materials this is initially less than the velocity of propagation of strains. The inertia wave will therefore travel within the plastic wave at an increasing velocity as the increased stress states overtake it (A_1, figure 4). If the stress-strain relation for the material is such that the velocity of the inertia wave equals the velocity of strain propagation at some

Downloaded from rsta.royalsocietypublishing.org

particular strain, the inertia wave will finally travel within the plastic wave at a constant velocity.

When the plastic wave is reflected at the centre of the wire (D) it is slowed down. The wave is now travelling through material that has been strained twice, by the incident and reflected plastic waves. It is also travelling through material which is itself moving towards the centre. The inertia wave, however, is unaffected by the movement of the material of the wire and is accelerated due to the increase in stress only (A_2).

Any element in the plastic wave travels away from the ends of the wire with a velocity V (L_1). When this wave has passed the element no further straining takes place between it and the fixed end so that the particle is stationary relative to that end. A particle will start to move again when passed by the reflected plastic wave travelling towards the end of the wire (L_2). The plastic wave continues to move along the wire until at some stage the restraint at the end falls and the stress within the wave is reduced by the elastic unloading waves. Since the velocity of elastic waves is approximately one hundred times that of the plastic waves and the interaction of the two is very complicated, no attempt has been made to depict the fading on the wave diagram.

The effect of the wave motion on the transverse deflexion of the wire depends on how the plastic strain wave modifies the action of the inertia wave. The deflexion of the centre is the sum of the deflexion caused by the inertia wave and the integral of the vertical components of strain along the deformed section of the wire. Hence the transverse velocity of the centre will depend upon the time rate of change of these two. Once the plastic wave has been formed the rate of change of elongation remains almost constant and the velocity component due to the plastic wave is fixed. The main change in velocity is therefore caused by the inertia wave, and the rate at which the central transverse velocity reaches its peak value depends upon the time taken for the inertia wave to reach the centre. The rate of the subsequent decrease in velocity depends upon the time it takes the reflected wave to return to the ends. As can be seen from the wave diagram shown in figure 4 the time of travel of the incident wave is considerably longer than that of the reflected wave and therefore the centre of the wire will decelerate more rapidly than it accelerated.

To summarize, the generation of the plastic strain wave is governed by the initial movement of the central section, That is, the strength of the wave will bear a direct relation to the initial acceleration. This in turn affects the velocity of the inertia wave which makes the major contribution to the central deflexion. It can be seen from this discussion that the time scale of the movement is not a function of the properties of the material alone but depends to a large extent on the initial rate at which the centre is made to deflect.

Cristescu (1961) and Craggs (1954) have shown that equations similar in form to (2·7) and (2·8) derived for the general case of motion of elastic-plastic wires can be solved using the method of characteristics. The types of waves represented by the characteristic equations have velocities

$$\left.\begin{aligned} C_1 &= \pm\sqrt{(\sigma_x/m)}, \\ C_2 &= \pm\sqrt{\left\{\frac{1}{\xi^2}\frac{\mathrm{d}(\sigma_x/m)}{\mathrm{d}(1/\xi^2)}\right\}} = \pm\sqrt{\frac{\mathrm{d}(\sigma_x/m)}{\mathrm{d}\epsilon_x}}, \end{aligned}\right\} \tag{4·10}$$

(since $\epsilon_x = -2\ln\xi$), where C_1 is the velocity of a transverse wave and C_2 is the velocity of a longitudinal wave. These waves are identical with those discussed above, being the inertia

Downloaded from rsta.royalsocietypublishing.org

and stress waves, respectively. Cristescu suggests two methods for the approximate integration of the equations of motion along these characteristics the simplest of the two involving the assumption that $C_1 = C_2$.

4·2. *The dynamic deflexion of a disk*

It has been shown in §4·1 that the equations of motion for a wire can be solved. The extension of this solution to the disk is not so simple. The introduction of bi-axial states of stress and strain, which determine the velocity of the plastic strain waves through the disk, excludes the use of the same techniques. If, however, strain hardening effects are ignored the analysis reduces to the determination of the inertia wave as described by Kirkwood & Richardson (1944). Then, by analogy with the wire, it should be possible to calculate the deformation of real materials possessing strain hardening plastic properties if the velocity of the strain wave was known.

If the change in disk thickness is assumed negligible and strain hardening is neglected, the stress everywhere will have the single value, σ_0, the yield stress. Then equation (2·13) simplifies to

$$-\frac{\partial^2\omega}{\partial\tau^2} = -\frac{\sigma_0}{p_0}\frac{1}{\eta}\frac{\partial}{\partial\psi}\left(\eta\frac{\partial\omega}{\partial\psi}\right) + \frac{p}{p_0}\frac{\partial\nu}{\partial\psi}, \tag{4·11}$$

where $p_0 = P_0 R/\bar{h}$ and P_0 is the magnitude of the suddenly applied pressure load. The initial conditions are: at $\tau = 0$; $p = 0$, ω and $\partial\omega/\partial\tau = 0$. The boundary conditions are: at $\tau \geqslant 0$: $p = p_0$ and $\omega = 0$ at $\psi = 1$

and the solution is $$-\omega = \tfrac{1}{2}\tau^2 \quad \text{when} \quad \psi \leqslant (1 - a_0\tau) \tag{4·12}$$

and $$-\omega = \frac{1}{2}\left\{\tau^2 - \frac{1}{\psi^{\frac{1}{2}}}\left(\tau - \frac{1-\psi}{a_0}\right)^2\right\} \quad \text{when} \quad \psi \geqslant (1 - a_0\tau), \tag{4·13}$$

where $$a_0^2 = \sigma_0/p_0.$$

Equation (4·11) differs from that obtained for the wire by the term $\sigma_0/p_0(1/\eta)\,\partial\omega/\partial\psi$. This term is introduced into the equation of motion when considering the forces acting in an element in the radial direction. Since the element approximates in shape to a trapezium, the force acting in one direction is greater than the opposing force by a factor involving the increase in arc length, $\mathrm{d}r\,\mathrm{d}\theta$. In other words, this term expresses the three-dimensional nature of the disk.

The solution is similar to that for the wire in that the transverse or inertia wave has a velocity given by $a_0 = \sqrt{(\sigma_0/p_0)}$ and the central movement is equivalent to the acceleration of a free body subjected to sudden loading.

Once the inertia wave reaches the centre of the disk at $\tau = 1/a_0$ the analysis breaks down and new boundary conditions must be applied. The disk could be assumed to be brought to rest by a retarding wave in a manner similar to that for the wire. The inaccuracy of such a solution has been indicated already and it is not attempted here.

If the strain hardening effects are included the propagation of strain waves must be considered. Craggs (1952) has attempted an analysis of the propagation of strain waves in circular membranes and shows that the velocity can be calculated from the equations of

Downloaded from rsta.royalsocietypublishing.org

motion, plasticity and strain-displacement. He shows that, in the elastic case the one-dimensional strain velocity for a wire, given by

$$C_E = \sqrt{\left(\frac{1}{\rho}\frac{d\sigma_x}{d\epsilon_x}\right)}$$

must be multiplied by the factor $[1-\lambda^2]^{-\frac{1}{2}}$,

where λ is Poisson's ratio, to give the radial strain velocity.

A similar modification for bi-axial states in the plastic region is required. A simple multiplication factor cannot be used and the complete analysis must be performed. Hence the scheme outlined for the wire cannot be used here. However, the analogy is reasonably close and similar conclusions can be drawn. If the equations (2·12) and (2·13) are rearranged by introducing the term $B^2 = \xi\eta$, we have

$$B^2\frac{\partial^2 v}{\partial\tau^2} = \frac{\partial}{\partial\psi}\left(B^2\frac{\sigma_r}{p_0}\frac{\partial v}{\partial\psi}\right) + \frac{B^2}{\xi}\frac{\partial\omega}{\partial\psi} - \frac{\sigma_\theta}{p_0}\xi \tag{4·14}$$

and

$$-B^2\frac{\partial^2\omega}{\partial\tau^2} = -\frac{\partial}{\partial\psi}\left(B^2\frac{\sigma_r}{p_0}\frac{\partial\omega}{\partial\psi}\right) + \frac{B^2}{\xi}\frac{\partial v}{\partial\psi}. \tag{4·15}$$

If these are compared with equations (2·7) and (2·8) it can be seen that they are of the same form with

$$B \equiv \xi$$

and

$$\sigma_r/p_0 \equiv \sigma_x/m$$

but include a term $\sigma_\theta\xi/p_0$ involving the circumferential stress. Hence it could be surmised that the deformation takes place in a manner similar to that of the wire and the velocities of the inertia and plastic strain waves would be approximated by

$$C_1' = \pm\sqrt{(\sigma_r/p_0)} \quad \text{and} \quad C_2' = \pm\sqrt{\frac{\mathrm{d}(\sigma_r/p_0)}{\mathrm{d}E_r}},$$

where

$$E_r = -2\ln B$$

(compare equations 4·10). Under the conditions mentioned above, the maximum stress and strain are in the radial and normal directions respectively so that the decisive stress-strain criterion requires

$$\sigma_r = f(-\epsilon_z).$$

However

$$\xi = \exp(\epsilon_z), \quad B = \eta\exp(2\epsilon_z)$$

so that B and hence E_r are functions of both strain and position.

Thus it is conceivable that similar techniques can be applied to both wire and disk, but that in the latter case the position of the element must be considered. Although a solution has not been attempted an inspection suggests that the deflexion of the disk will depend to a very large extent on its initial movement. That is, for a given material the deformation will depend upon the magnitude of the pressure loading and the corresponding initial acceleration of the disk.

5. Experimental

5·1. *Equipment*

A disk can be subjected to a sudden pressure loading by using a shock tube. This consists of a tube of uniform cross-section divided into two compartments by a diaphragm. Initially one compartment contains gas at high pressure and the other gas at ambient pressure and the system is in thermal equilibrium. When the separating diaphragm is ruptured a

Downloaded from rsta.royalsocietypublishing.org

state of disequilibrium is set up and the wave formation shown in the x-t diagram in figure 6 is generated. Assuming the diaphragm disintegrates instantaneously at time $t = 0$, a plane shock wave followed by a contact surface is transmitted into the low-pressure section and a rarefaction wave is simultaneously propagated into the high-pressure section.

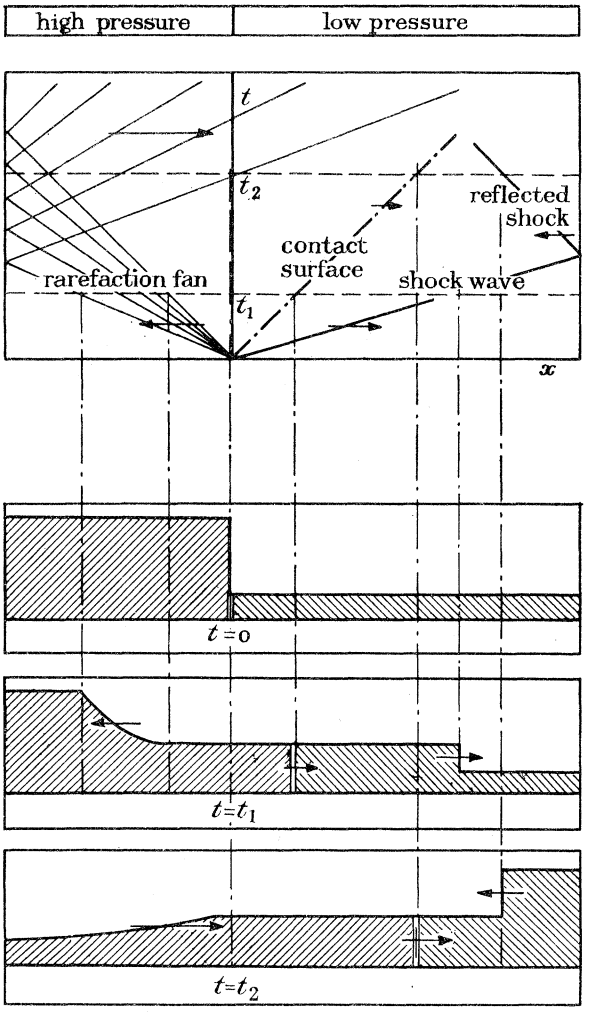

FIGURE 6. Wave formation and pressure distribution in shock tube.

The low-pressure gas is initially stationary and the shock consists of a discontinuity of pressure, temperature and particle velocity travelling through it. When the shock is reflected off the fixed end of the tube the gas is brought suddenly to rest and an instantaneous increase in pressure is obtained. The pressure remains constant until some disturbance is generated by the interaction of the contact surface and either the reflected shock or the reflected rarefaction wave.

The contact surface defines the boundary between the gas initially in the low-pressure section, which is being compressed, and that in the high-pressure section, which is being expanded. Hence there is a discontinuity of temperature in this plane but the velocities and pressures in the two gases are identical.

Shock tube theory (Glass, Martin & Patterson 1953) has been developed to describe the phenomenon precisely. For a given initial pressure ratio across the diaphragm the

Downloaded from rsta.royalsocietypublishing.org

magnitude and duration of the pressure loading on the closed end of the shock tube can be calculated for different tube lengths and the apparatus can be designed to cope with time intervals involved with disk deflexion over a range of pressure loads. The pressure loading is calculated from

$$p_{51} = \frac{\alpha + 2 - p_{12}}{(1 + \alpha p_{12})\, p_{12}} \tag{5·1}$$

and

$$p_{14} = p_{12}\left\{1 - \left(\frac{1}{p_{12}} - 1\right)\left(\frac{\beta}{(\alpha/p_{12}) + 1}\right)^{\frac{1}{2}}\right\}^{1/\beta}, \tag{5·2}$$

where

$$\alpha = \frac{\gamma + 1}{\gamma - 1}, \quad \beta = \frac{\gamma - 1}{2\gamma},$$

$$p_{51} = \frac{P_5}{P_1} = \frac{\text{pressure loading}}{\text{initial pressure}},$$

$$p_{41} = \frac{P_4}{P_1} = \frac{\text{high pressure}}{\text{initial pressure}},$$

$$p_{12} = \frac{P_1}{P_2} = \frac{\text{initial pressure}}{\text{pressure behind shock}},$$

$$\gamma = \text{ratio of specific heats.}$$

The duration of the constant-pressure load at the closed end depends upon the shock-tube pressure ratio, p_{41}, and the lengths of the high- and low-pressure sections of the shock tube. Changing these three parameters alters the system of waves generated in the tube and in particular alters the interaction of the system with the reflected shock wave. These interactions are illustrated in figure 7. The diagrams show three shock tubes which have high-pressure sections of the same length and are operated at the same pressure ratio but with low-pressure sections of increasing length. In the first case (a) the reflected shock wave meets the contact surface first and a second shock is produced which reaches the closed end a time Δt_R after the first shock wave reflexion. In the third case (c) the reflected rarefaction wave is diffracted at the contact surface before interacting with the reflected shock wave. The disturbance at the closed end, which occurs a time Δt_R after the initial shock-wave reflexion, is the twice diffracted rarefaction wave. The second case (b) represents the intermediate case, which we have termed triple interaction, in which all three waves interact at the same time.

The duration of pressure loading can be assumed to be at least equal to the time interval Δt_c as long as the region LMN on the wave diagram is undisturbed by any waves. Δt_c is a function of p_{21} and $x_{\text{l.p.}}$, the length of the low-pressure section, so that the constant pressure duration can be plotted against p_{21} for several values of $x_{\text{l.p.}}$ as long as provision is made to discount pressures and tube lengths at which the wave formations shown in figure 7 (b) and (c) occur.

Triple interaction occurs when the low-pressure length is given by

$$X = \left[\tau_c + \frac{X_c}{W_{21}}\right] \Big/ \left[\frac{1}{W_{11}} + \frac{1}{W_{21}}\right], \tag{5·3}$$

PHILOSOPHICAL TRANSACTIONS OF THE ROYAL SOCIETY A MATHEMATICAL, PHYSICAL & ENGINEERING SCIENCES
PHILOSOPHICAL TRANSACTIONS OF THE ROYAL SOCIETY A MATHEMATICAL, PHYSICAL & ENGINEERING SCIENCES

Downloaded from rsta.royalsocietypublishing.org

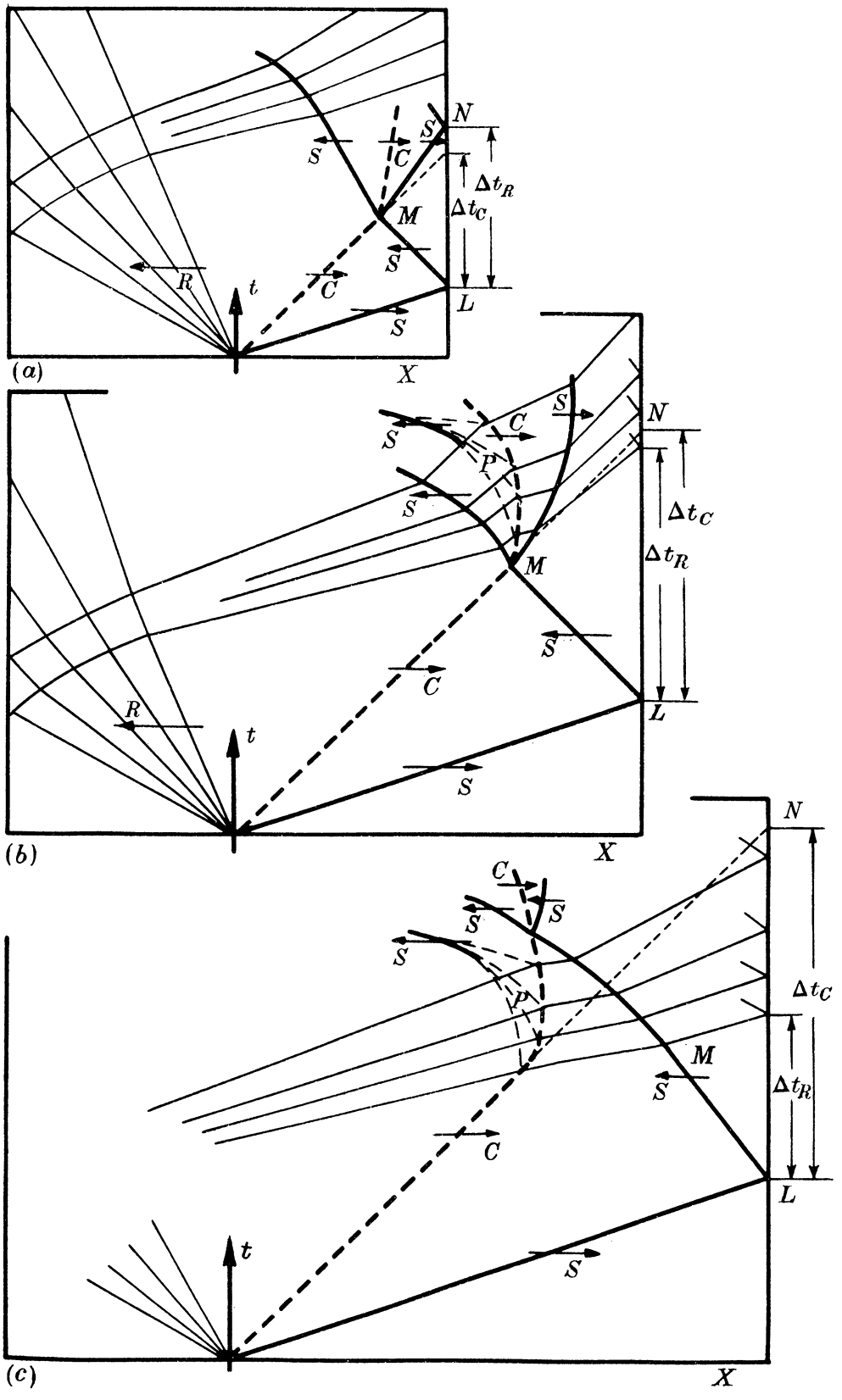

FIGURE 7. The effect of low-pressure section length on wave interaction. *S*, shock wave; *C*, contact surface; *R*, rarefaction fan; *P*, compression fan.

PHILOSOPHICAL TRANSACTIONS OF THE ROYAL SOCIETY A MATHEMATICAL, PHYSICAL & ENGINEERING SCIENCES
PHILOSOPHICAL TRANSACTIONS OF THE ROYAL SOCIETY A MATHEMATICAL, PHYSICAL & ENGINEERING SCIENCES

Downloaded from rsta.royalsocietypublishing.org

where

$$X = x_{\text{l.p.}}/x_{\text{h.p.}},$$

$$\tau_c = 2p_{34},$$

$$X_c = 2(\alpha-1)(1-p_{34}^{\beta})\,p_{34}^{-\frac{1}{2}\alpha\beta},$$

$$W_{21} = \frac{2+(\alpha-1)\,p_{12}}{[(\alpha+1)\,(\alpha+p_{12})\,p_{12}]^{\frac{1}{2}}},$$

$$W_{11}^2 = \beta(1+\alpha p_{21}) \quad \text{and} \quad p_{34} = p_{14}\,p_{21}.$$

X therefore depends on the pressure ratio p_{14} only and as $p_{14} \to 1$, $X \to 1$.

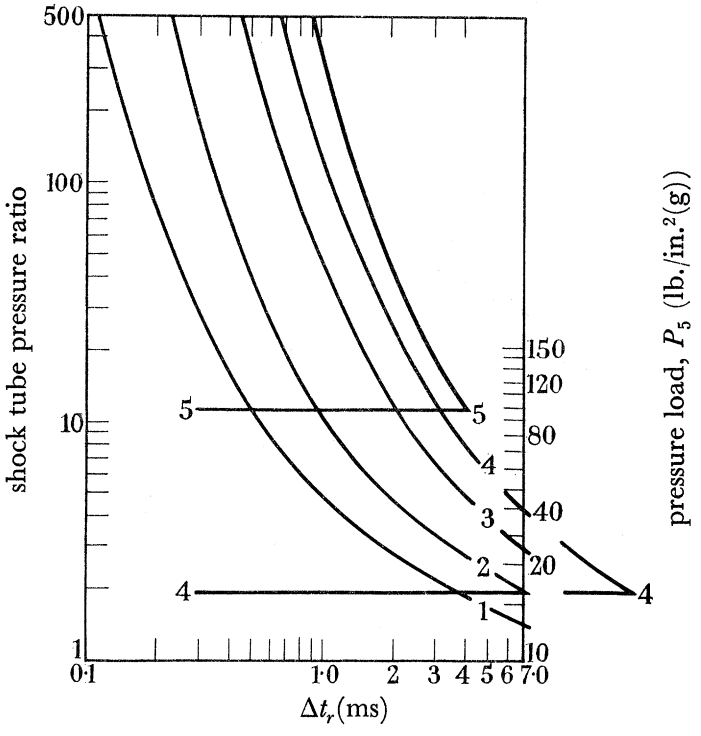

FIGURE 8. Shock-tube performance. The low-pressure section lengths in feet are indicated on the curves.

Figure 8 has been constructed on this basis to represent the field of application of a shock tube in terms of the pressure ratio p_{41}, the duration of constant pressure at the tube end, Δt_r, and the tube length. Thus an operating point lying on the curve for a given low-pressure length and above the critical pressure for triple interaction will represent the shock-tube pressure ratio required to produce a given pressure load P_5 with a duration at least equal to Δt_r.

(*a*) *The shock tube*

The shock tube is illustrated in figure 9. The high-pressure section is 6 ft. long and the low-pressure section 4 ft. and both are made out of 6 in. internal diameter steel tubes as specified by B.S. 1378. Flanges 12 in. in diameter by $1\frac{1}{8}$ in. thick are expanded on to the four ends in accordance with B.S. 1740. The assembly has been hydraulically tested up to 700 lb./in.^{2} (g). The dimensions have been dictated by considerations of space, but the low-pressure section can be lengthened without reducing the effectiveness of the design.

Downloaded from rsta.royalsocietypublishing.org

Pairs of windows are fitted in the low-pressure section at points B_1 and B_2 and two bosses have been welded on at A. The windows are used to time the passage of the shock and provide a signal for triggering the equipment used to examine the deflexion of the disk. The bosses at A are fitted with insulated terminals and a resistance wire is attached between them inside

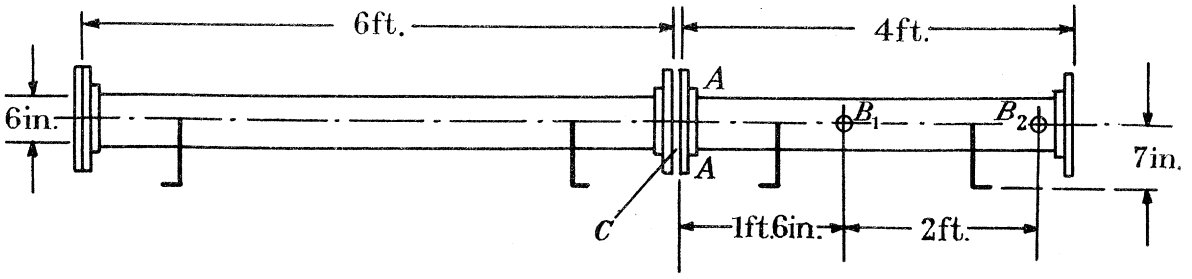

FIGURE 9. Shock tube.

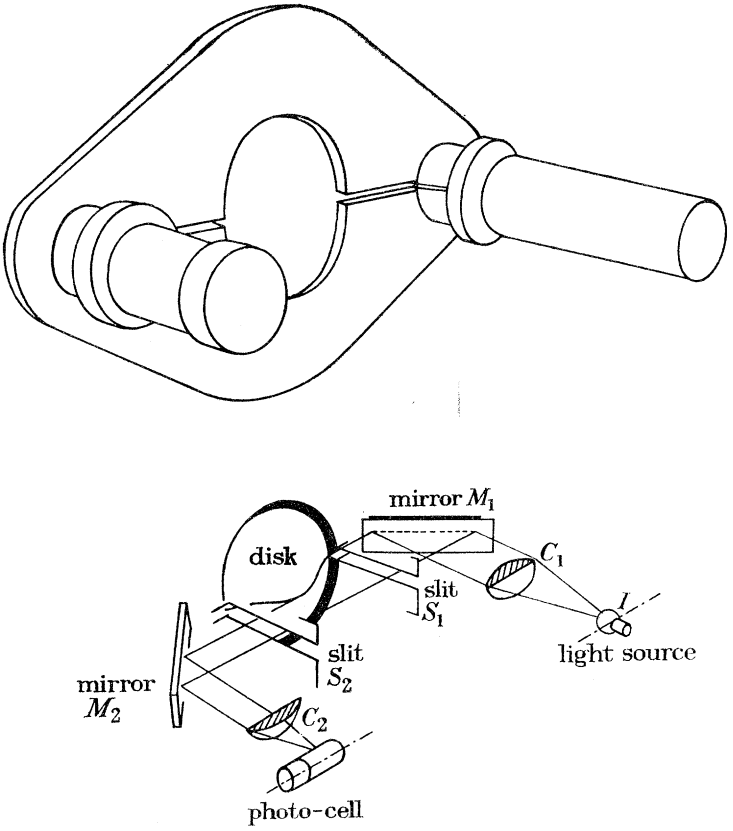

FIGURE 10. Deflexion gauge, perspective drawing.

the tube. The wire is placed so that it touches the diaphragm separating the two sections and it is heated by an electrical current to break the diaphragm at the required pressure.

The separating diaphragm which is made of cellulose acetate is held in a capsule which is mounted between the two tubes and its design is similar to that used in commercial bursting disk holders.

Downloaded from rsta.royalsocietypublishing.org

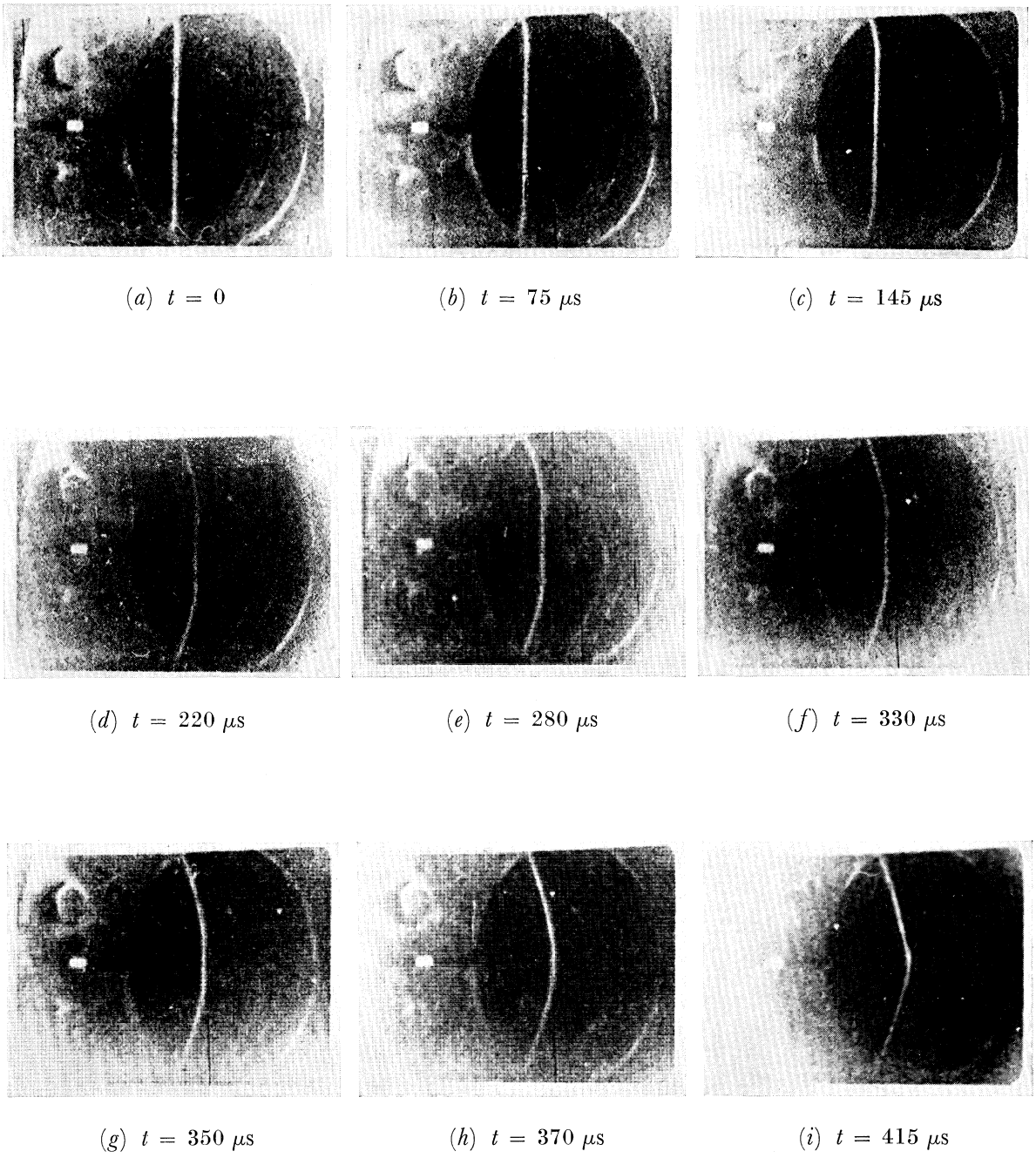

(*a*) $t = 0$ (*b*) $t = 75\ \mu s$ (*c*) $t = 145\ \mu s$

(*d*) $t = 220\ \mu s$ (*e*) $t = 280\ \mu s$ (*f*) $t = 330\ \mu s$

(*g*) $t = 350\ \mu s$ (*h*) $t = 370\ \mu s$ (*i*) $t = 415\ \mu s$

FIGURE 12. High-speed ciné recordings of 6 in. diameter copper disk, 0·0027 in. thick (*ca.* 200 000 pictures per second; approximate time intervals in microseconds).

(*Facing p.* 20)

PHILOSOPHICAL TRANSACTIONS OF THE ROYAL SOCIETY A MATHEMATICAL, PHYSICAL & ENGINEERING SCIENCES

PHILOSOPHICAL TRANSACTIONS OF THE ROYAL SOCIETY A MATHEMATICAL, PHYSICAL & ENGINEERING SCIENCES

Downloaded from rsta.royalsocietypublishing.org

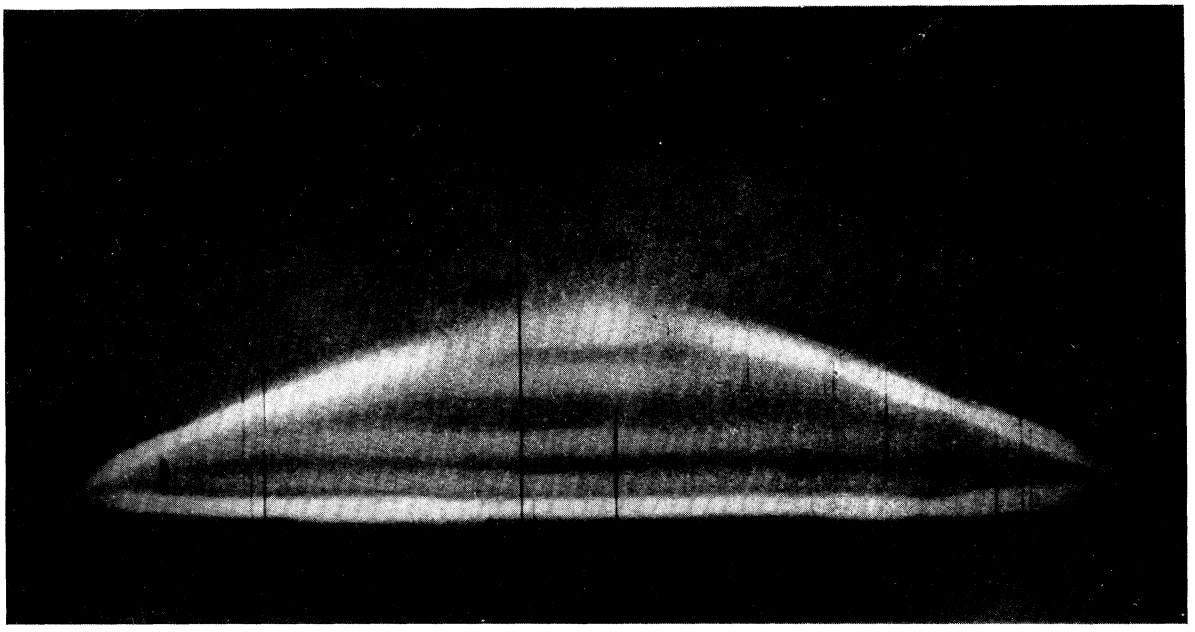

FIGURE 13. Multiple flash photograph of 4 in. diameter copper disk, 0·002 in. thick.

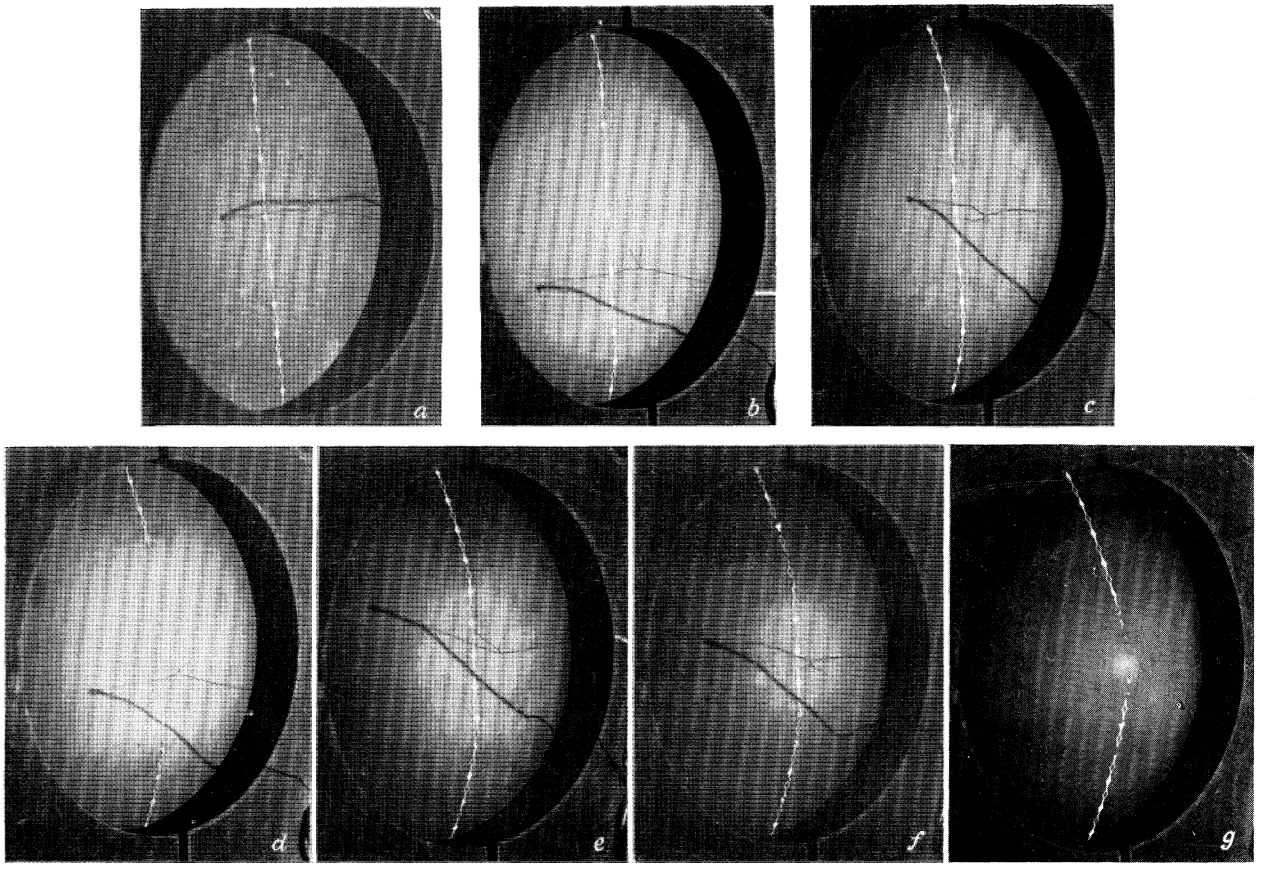

FIGURE 14. Single flash photographs of 6 in. diameter copper disk, 0·002 in. thick.

PHILOSOPHICAL TRANSACTIONS OF THE ROYAL SOCIETY A MATHEMATICAL, PHYSICAL & ENGINEERING SCIENCES

PHILOSOPHICAL TRANSACTIONS OF THE ROYAL SOCIETY A MATHEMATICAL, PHYSICAL & ENGINEERING SCIENCES

Downloaded from rsta.royalsocietypublishing.org

PHILOSOPHICAL TRANSACTIONS OF THE ROYAL SOCIETY A MATHEMATICAL, PHYSICAL & ENGINEERING SCIENCES

(*b*) *Deflexion measurement*

The deflexion of the test disk on the impact of the shock wave was examined by two methods. The central deflexion was measured electronically by the use of a beam of light and a photocell, and photographic records were made of the changing shape of the disk.

To measure the central deflexion while the pressure is applied, the disk must be held on the end of the shock tube and the position of its centre recorded continuously. A perspective drawing (figure 10) of the deflexion gauge head indicates the optical method employed. A light beam produced by a source, I, and a condenser, C_1, is reflected from a mirror, M_1, through a slit, S_1, and across the face of the test disk. The beam then enters a second slit, S_2, is reflected from a second mirror, M_2, into a condenser, C_2, to be focused on a screen. A photomultiplier observes the image of the first slit on the screen. As the disk deflects the light beam is partly obscured and the output from the photomultiplier is reduced proportionally with the disk deflexion. The output from this is fed direct to a Solatron (type CD 513) oscilloscope and the trace, produced by the changing light intensity, photographed. The oscilloscope time base was triggered from the second pair of windows in the shock tube.

The test disk holder, shown in figure 11, was designed to minimize the extent to which the disk was obscured. The clamping plate, *RR*, is split in two and the disk, *D*, is held in the backing plate, *BP*, by a thin ring, *SR*, which applies an even pressure over the entire rim of the disk. This ring is only $\frac{1}{8}$ in. thick and provides the only obstruction to the light beam used in measuring the deflexion. The inner edge (point *b* in the drawing) of this ring is radiused to prevent it cutting the disk and causing shear at the edges. The mirrors, light source and photomultiplier are housed in tubes fitted to the face plate, *FP*, which holds the disk assembly onto the open end of the shock tube. Three assemblies have been made so that disks of 2, 4 and 6 in. diameters can be tested.

Further information on the deflexion history of the disk was established photographically by using cinematographic, multiple image and single flash methods. Owing to the visual obstruction of the disk by the clamping plate the photographs were taken at an angle to the tube. The disk was blackened and a white line painted along its vertical diameter to give a clear picture of the profile.

A Courtney-Pratt high-speed camera, was used to obtain records for observational purposes; a sequence of photographs taken from such a record is shown in figure 12, plate 1. The sampling technique used in this camera requires a lens which moves relative to both the photographic plate and the object, and hence the recorded image appears to have an additional movement which introduces a change of perspective for each picture. This distortion makes measurements difficult and to supplement these photographs a flash system was devised whereby a true record of the deformation could be determined.

A series of flashes of short duration illuminates the face of the disk and, by means of a lens, produces a multiple image on a stationary film. This process is carried out in the dark and the flash is triggered to coincide with the initial movement of the disk. The flash source consists of a Ferranti cathode-ray tube (type CL 73) running at 25 kV and held at cut-off by a battery grid bias. A short train of pulses, initiated by the trigger, is fed to the grid. The face of the c.r.t. is illuminated for the duration of each pulse and parabolic mirror focuses the light on the disk. Ilford HPS film and an f/1·0 lens enabled a record of sufficient intensity

Downloaded from rsta.royalsocietypublishing.org

to be made. The electronic equipment is briefly described by Munday & Tyley (1958). An example of the multiple image photograph is shown in figure 13, plate 1. The true deflected shape of the disk shown in figure 15 was obtained from the multiple-flash photograph by setting up the camera with a light source so that an image was projected on to a plane in the axis of the tube and at the same angle from which the negative was obtained.

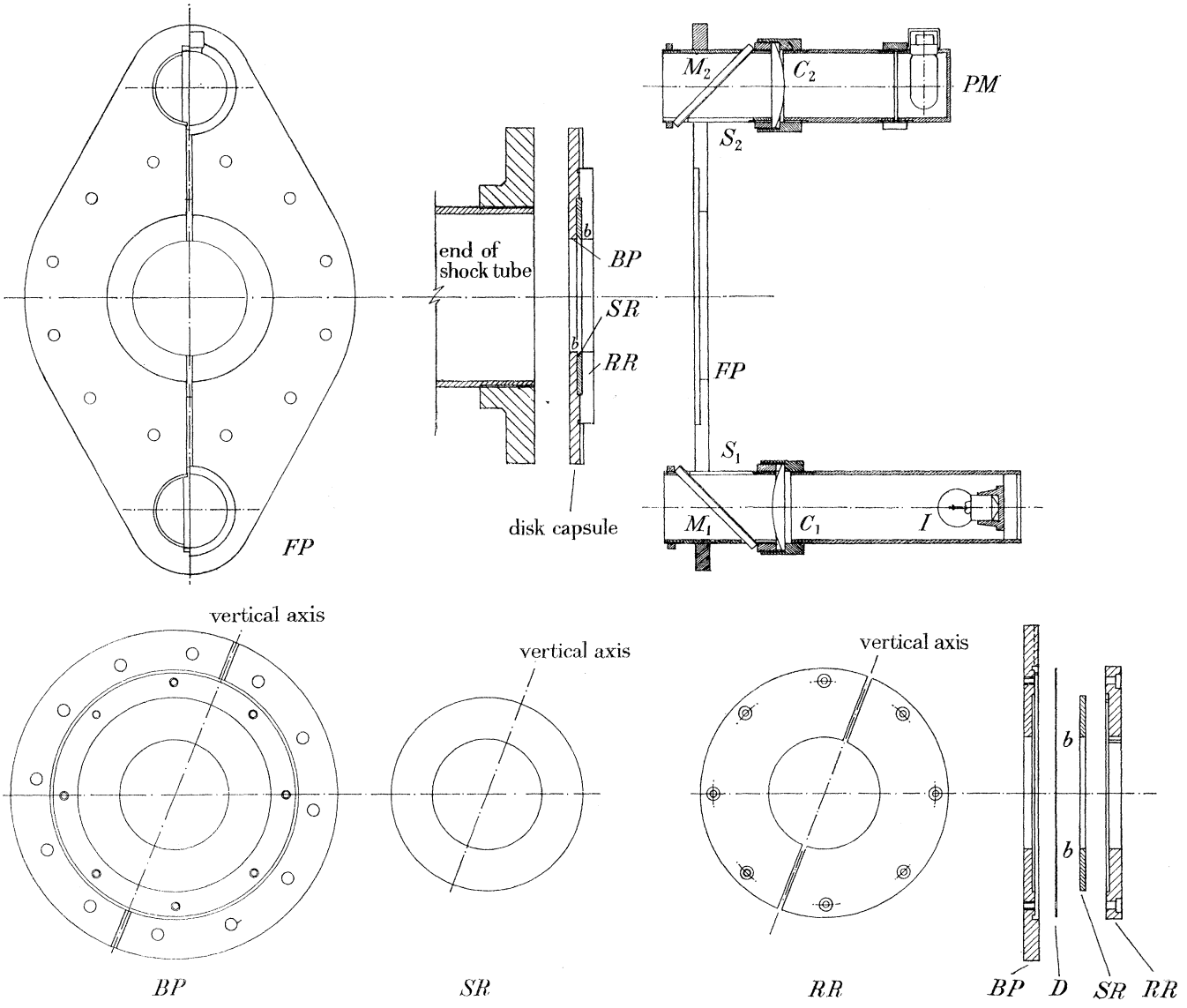

FIGURE 11. Detailed design of deflexion gauge and disk holder.

The correct angle was determined by adjusting the angle of projection until the image of the edge of the flat part of the disk exactly coincided with a circle of the same diameter drawn on a sheet of paper held perpendicular to the plane of projection. The deflected positions were traced out and a final check on the accuracy of the projection made by comparing the final position with the true shape of the deformed disk. Figure 16 shows the experimental arrangement for taking the photograph and illustrates how the projection was obtained.

The photographs in figure 14, plate 2, were taken from a series of experiments in which similar disks were loaded to the same pressure. A spark, initiated by the contact made

Downloaded from rsta.royalsocietypublishing.org

between the disk and a fine wire probe, illuminated the disk. The camera shutter was permanently open so that the instant of exposure could be chosen to coincide with a given displacement of the disk.

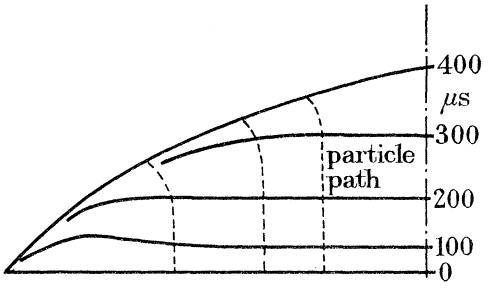

FIGURE 15. Disk deflexion as projected from figure 13.

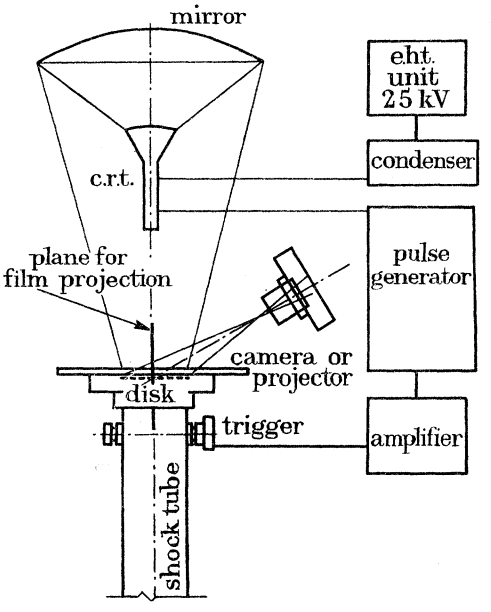

FIGURE 16. Equipment for multiple flash photograph.

(*c*) *Disk material*

The shock tube design permits the dynamic testing, to bursting pressure, of copper disks up to 6 in. in diameter and up to 0·008 in. thick. To obtain a maximum loading area over the full diameter a 9 in. width foil is required. The only material available in the smaller thickness ranges was an electro-deposited copper foil, manufactured by the Royal Mint Refinery, which is specified as of uniform thickness to close limits across the width and hardness equivalent to rolled copper sheet. The thickness, as represented by the mass per unit area figure of 0·735, 1·470 and 2·000 oz./ft.^{2}, are nominally 0·001, 0·002 and 0·0027 in. respectively. Deviations of up to 4% were found and the actual thicknesses were 0·0013, 0·0024 and 0·0032 in. All the disks were closely packed in containers and annealed to 500 °C.

5·2. *Performance of equipment*

All but one of the preliminary experiments discussed here were performed with a shock tube pressure ratio of 2·88. The propagation of shock wave, contact surface and rarefaction wave at this pressure have been calculated and are plotted on the wave diagram in figure 17.

Downloaded from rsta.royalsocietypublishing.org

The shock wave, S and the contact surface, C, travel at velocities 1300 and 430 ft./s, respectively. The rarefaction wave, R, travels through the high-pressure section with a leading velocity of 1100 ft./s and is reflected from the end but does not interfere with the region of constant pressure. This is terminated by the shock wave reflected at the contact surface.

The loading pressure is 24·7 lb./in.^{2} (g) and its duration is 8 ms which, as the results show, is more than sufficient for the full deflexion of the disk. The calculation of the magnitude of the pressure behind the reflected shock wave is based on the assumption that the

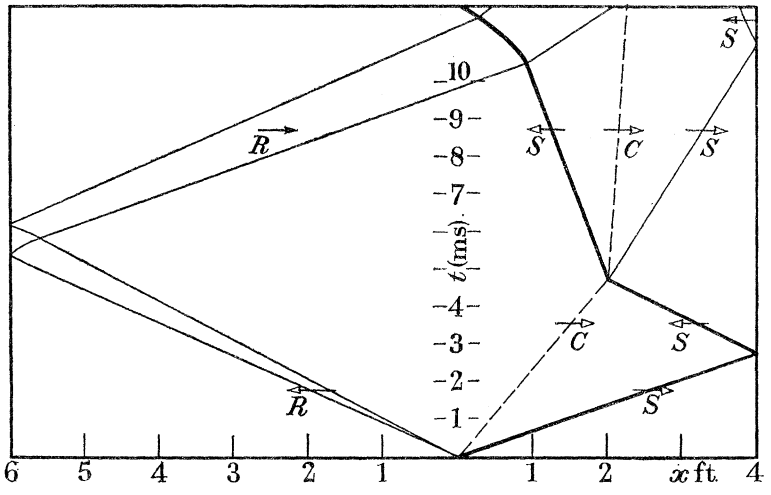

FIGURE 17. Wave system in shock tube at a pressure ratio of $p_{41} = 2{\cdot}88$.

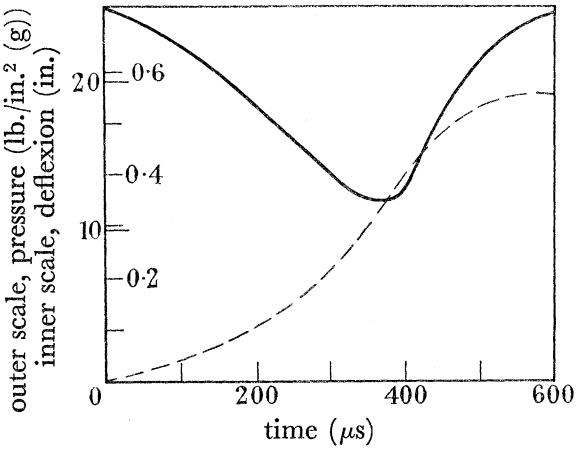

FIGURE 18. Pressure fall due to disk movement. ———, Pressure difference across disk; – – –, central deflexion. 4 in. diameter × 0·002 in. thick copper disk loaded to 24·7 lb./in.^{2} (g).

kinetic energy of the moving gas is all converted to pressure energy as the gas is brought to rest at the wall. In the case of a deflecting disk this is not so and, if the velocity of the disk is comparable with the velocity of sound in air, the pressure will fall. Results show that the disk centre moves at a speed of about one-quarter of the speed of sound in air and it has been necessary to determine the effect of this movement of the constant pressure load. Meyer (1957) has investigated the impact of shock waves on a free wall and has shown that the pressure difference across the wall can be calculated. Using a simplification of Meyer's

Downloaded from rsta.royalsocietypublishing.org

theory to give an approximate measure of the loading, the experimentally recorded velocity of a disk has been used to calculate this fall in pressure, and the result is plotted in figure 18. In practice the pressure never falls as low as the calculated value since the entire cross-section of the disk is not moving at the velocity of its centre.

6. Results

The photographs shown in figures 12 to 14, plates 1 and 2 indicate that the disk deforms as described in the theoretical section, the central section of the disk remaining flat and a transverse discontinuity travelling in from the rim towards the centre. The movement of the centre of the disk is found to coincide with measurements made using the deflexion head as shown in figure 20 (*b*).

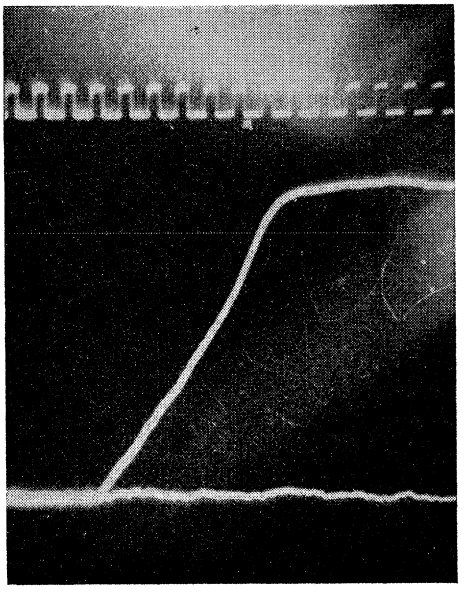

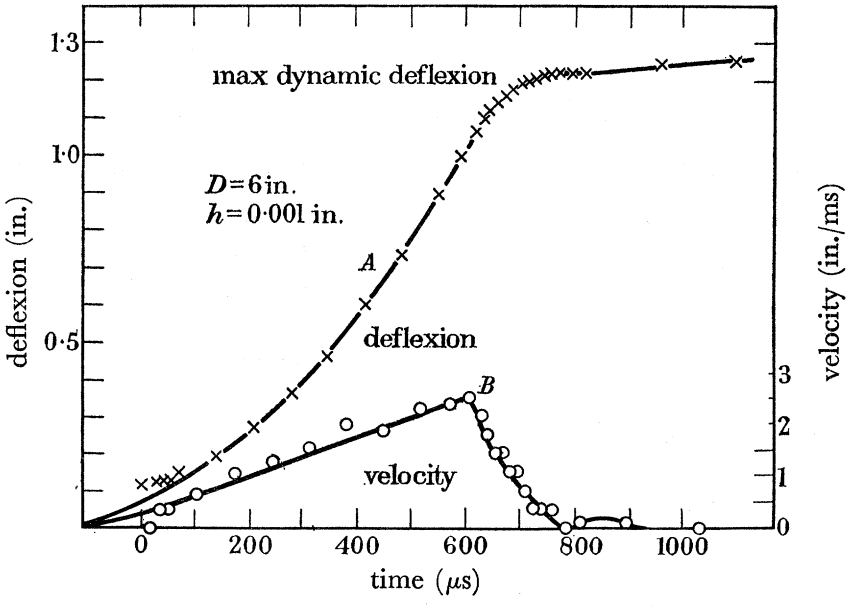

Figure 19. Oscilloscope record and measured values.

Downloaded from rsta.royalsocietypublishing.org

The measurement of the deflexion of the centre of the disk yields the most reliable quantitative information on the dynamic deformation. Table 1 lists data obtained from five experiments with disks of radius 2 and 3 in. A typical oscilloscope record from one of these experiments is shown in figure 19 together with the trajectory of the centre (curve A) and

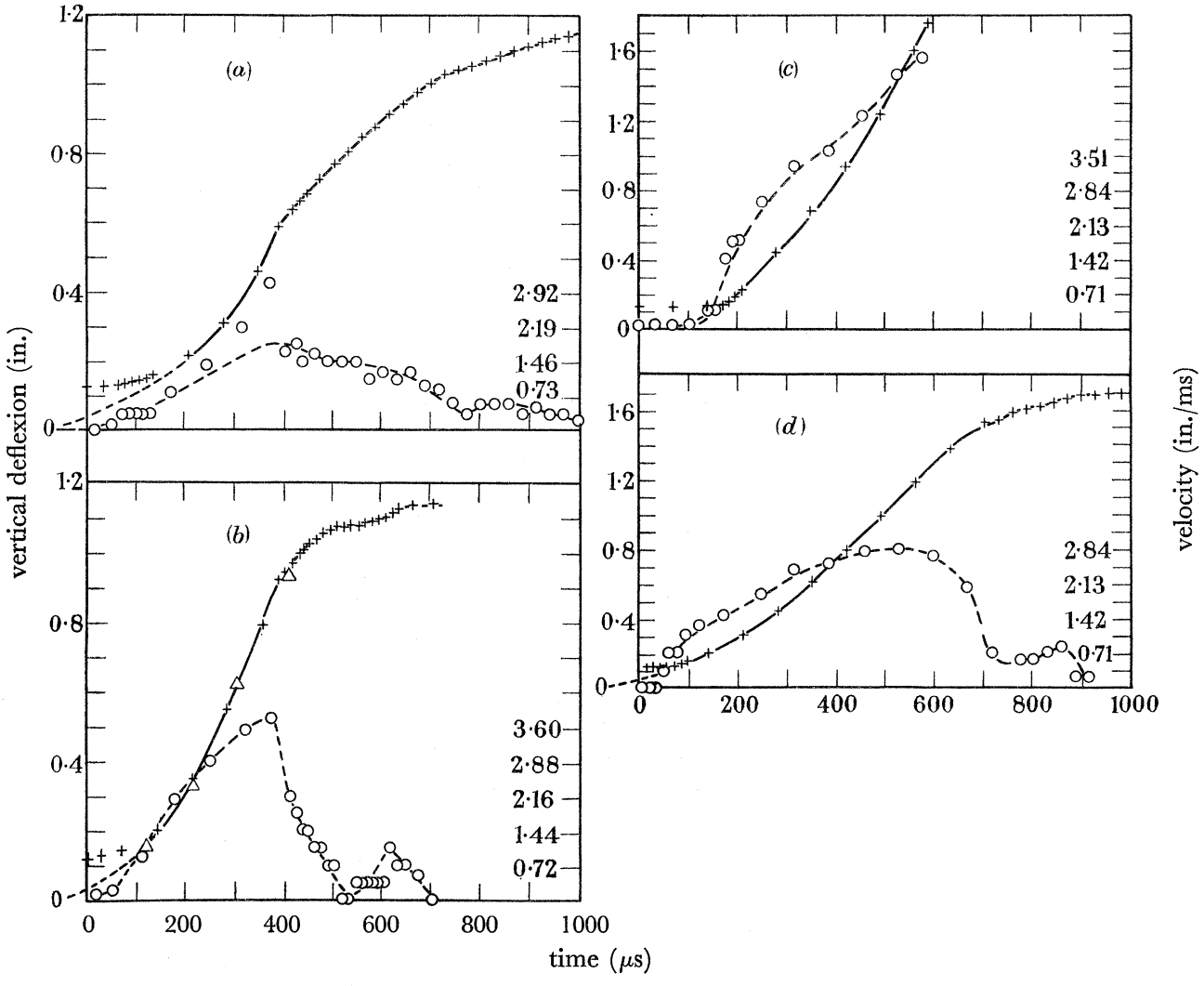

FIGURE 20. Deflexion and velocity plots for four disks. +, Deflexion; ○, velocity.

	run no.	R (in.)	$\bar{h}$ (in.)
(a)	A v	2	0·0027
(b)	A iv	2	0·002 (Δ multiple flash record)
(c)	A iii	2	0·001 (disk burst)
(d)	A i	3	0·0027

the variation of velocity (curve B) measured from it. Results from the other four experiments are shown in figure 20.

The individual experiments are correlated by the use of the dimensionless parameters

$$T = \sqrt{\left(\frac{A_0}{R}\right)}\, t, \quad z = \frac{W_0}{W_0^*} \quad \text{and} \quad v = \frac{V}{W_0^*}\sqrt{\frac{R}{A_0}},$$

Downloaded from rsta.royalsocietypublishing.org

where A_0 is the initial acceleration; W_0 the central deflexion; W_0^* the maximum dynamic central deflexion; and V is the velocity of the centre. The variation of deflexion and velocity as a function of time is shown in figures 21 and 22. It can be seen that a good correlation has been obtained.

As shown in figure 23 the shape of the disk in its final deformed position is almost identical for all the disks irrespective of thickness, diameter and loading. The co-ordinates have been

TABLE 1. DYNAMICALLY LOADED DISKS

run no.	radius (in.)	thickness (in.)		pressure load	initial acceleration in./(ms)^2		maximum velocity	final central deflexion (in.)	
		nominal	actual	(lb./in.^{2}(g))	measured	free plate	(in./ms)	W_0^*	equivalent equilibrium loading
A III	2	0·0010	0·0013	24·7	10·4	22·8	5·5	disk burst	0·746
A IV	2	0·0020	0·0024	24·7	9·2	12·4	3·7	1·14	0·502
A V	2	0·0027	0·0032	24·7	4·0	9·3	1·5	1·15	0·420
A I	3	0·0027	0·0032	24·7	6·1	9·3	2·9	1·69	0·538
A VI	3	0·0010	0·0013	8·82	5·3	8·1	2·5	1·24	0·500

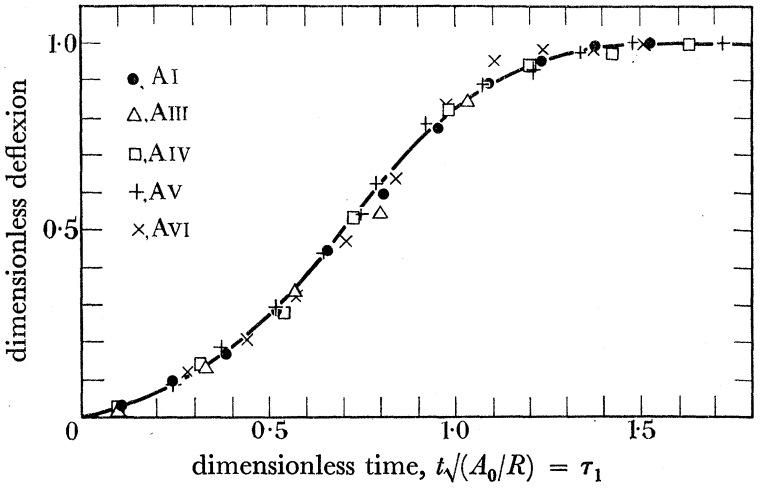

FIGURE 21. Correlation of disk deflexion.

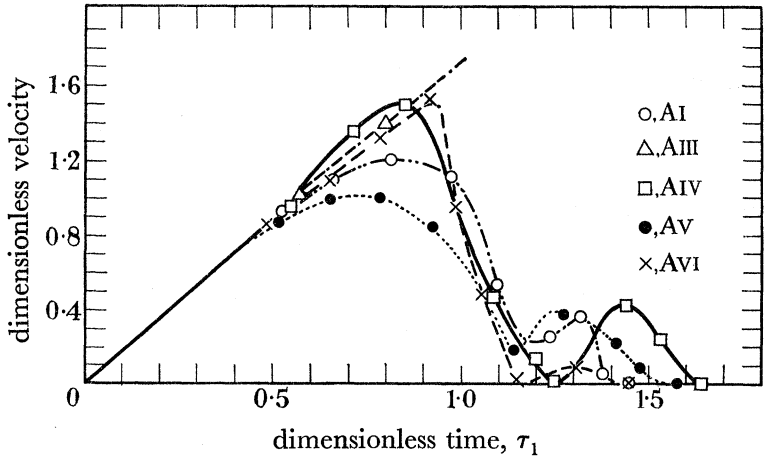

FIGURE 22. Correlation of disk velocity.

Downloaded from rsta.royalsocietypublishing.org

plotted in the dimensionless form W^*/W_0^* and η, where the asterisk represents the final position and the subscript 0 the pole of the disk. The relation between height and radial position is

$$W^*/W_0^* = 1-\eta^{\frac{3}{2}}. \tag{6·2}$$

W_0^*/R varies from 0·39 to 0·5 and appears to be directly related to the initial acceleration. The shape of a disk loaded slowly to a comparable pressure is also shown in this figure.

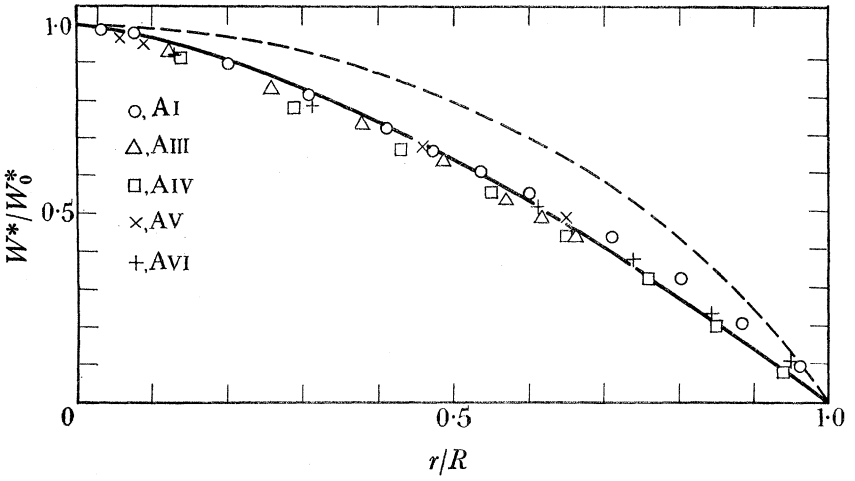

FIGURE 23. The disk profile after dynamic loading. ———, $W^*/W_0^* = 1-(r/R)^{\frac{3}{2}}$; – – –, equilibrium loading.

7. CONCLUSIONS

The theoretical considerations of the problem of dynamic deflexion of a disk leads to the conclusion that, for high rates of loading, two types of wave must exist to allow for the deformation. These are the plastic strain and inertia waves. The former enables the disk to stretch so that it may deform by a mechanism involving the latter. These two waves are interdependent but travel at different speeds which depend on the state strain in the material. The strain wave also affects the state of stress in the disk so that the nature of the interaction between the waves is some function of the many possible variables. While this implication makes it difficult to calculate the deflexion rate from the equations of motion the analysis does lead to a useful correlation of experiments for a particular material. Analogy with an extensible wire under similar conditions of loading suggests that the initial acceleration of the disk plays a controlling role and if it could be related to the stress-strain laws of the material the deflexion could be specified for all materials on a single curve.

In the experiments with annealed copper the discontinuity in curvature which marks the inertia wave during deformation is clearly seen. The velocity of the inertia wave, as measured from the photographs, varies from 3 in./ms near the rim to 7 in./ms at the centre. These values agree with theoretical predictions for a local strain increase from 0 to 0·3. It can be shown that local strains of this order of magnitude are required to produce the deformation observed.

Strain waves cannot be discerned in the photographs but their presence is implied by the nature of the motion of the disk, since the incident and reflected inertia waves have different velocities. The movement associated with the reflected wave is small and cannot be observed,

Downloaded from rsta.royalsocietypublishing.org

but the difference between the rates of acceleration and deceleration of the disk centre can only be explained by an increase in strain as shown in the wave diagram in figure 4. Further, the two rates can be measured from figure 22 and it is found that the reflected wave moves twice as rapidly as the incident one. Again this is in keeping with theoretical predictions since the velocity of the inertia wave is doubled by an increase of strain of about 0·3.

Quantitative information is given in the deflexion and velocity plots shown in figures 21 and 22. Their dimensionless nature suggests that the deflexion is dependent upon the initial acceleration and disk radius. Discrepancies towards the end of the deflexion process indicate that other factors are involved. At this stage it may be concluded that the rate of deformation of a copper disk is such that the initial acceleration is about half the theoretical value for the equivalent free plate.

The later stages of the disk deflexion cannot be perceived in the individual photographs shown in figures 12 to 14, but when the high-speed film records are projected the disk is observed to slow down and the centre appears to 'bounce' or oscillate. This oscillation is partially associated with the dip in the centre of the disk visible in figure 14 (*d*), but it is suggested that this is largely the result of further reflexions of the inertia wave. These reflexions account for the presence of the second velocity peak in figure 22.

The shape of the disk in its final deformed position is given by an equation which is identical with the theoretical one for the disk shape at the instant when the inertia wave reaches the centre. This equation has been obtained by an analysis in which strain-hardening effects have been neglected and hence it may be surmized that the inertia wave plays a major part in the deformation of the disk. The propagation of the plastic wave then only modifies the time scale of the process in some non-linear manner.

The aim of this work was to investigate the rate of deflexion of bursting disks used to protect industrial installations against the effects of rapid increase of internal pressure. The response of these disks to shock pressure loadings has been established and the mode of deformation described. It is suggested that the experimental techniques may well have importance in the field of plastic deformation at high rates of strain since they have certain advantages over orthodox methods. Straining rates in the range $10^5\ s^{-1}$ can be attained and the magnitudes of the strains to be measured are large. Similar techniques can also be used to determine the bursting pressure of disks under these conditions. Studies of rate of crack propagation and the dependence of failure on the velocity and therefore magnitude, of strain waves also lead to valuable information on the ultimate strength of materials.

The authors would like to thank J. Langham Thompson and Co., for the loan of a Courtney-Pratt high-speed sampling camera, and Mr L. R. Tyley for his assistance in much of the photographic work.

References

Brown, W. F. & Sachs, G. 1948 *Trans. Amer. Soc. Mech. Engrs.* **70**, 241.
Brown, W. F. & Thompson, J. A. 1949 *Trans. Amer. Soc. Mech. Engrs*, **71**, 575.
Craggs, J. W. 1952 *Proc. Roy. Soc. Edinb.* **63**, 359.
Craggs, J. W. 1954 *J. Mech. Phys. Solids*, **2**, 286.
Craggs, J. W. 1961 *Progress in Solid Mechanics, II*,
Cristescu, N. 1961 *J. Mech. Phys. Solids* **9**, 165.
Glass, I. I., Martin, W. & Patterson, N. 1953 *Inst. Aerophys. Toronto*, UTIA no. 2.

PHILOSOPHICAL TRANSACTIONS OF THE ROYAL SOCIETY A MATHEMATICAL, PHYSICAL & ENGINEERING SCIENCES
PHILOSOPHICAL TRANSACTIONS OF THE ROYAL SOCIETY A MATHEMATICAL, PHYSICAL & ENGINEERING SCIENCES

Downloaded from rsta.royalsocietypublishing.org

Gleyzal, A. 1948 *J. Appl. Mech.* **15**, 288.
Goldsmith, W. 1960 *Impact.* London: Arnold.
Hill, R. 1950 *Phil. Mag.* **41**, 1133.
Kirkwood, J. G. & Richardson, J. M. 1944 *Nat. Def. Res. Cttee. O.S.R.D. Rep.* no. 4200.
Kolsky, H. 1953 *Stress waves in solids.* Oxford University Press.
Mellor, P. B. 1956 *J. Mech. Phys. Solids*, **5**, 41.
Meyer, R. F. 1957 *J. Fluid Mech.* **3**, 309.
Munday, G. 1961 Ph.D. Thesis (London).
Munday, G & Newitt, D. M. 1962 *Society of Chemical Industry Symposium on High Pressure.* Society of Chemical Industry.
Munday, G. & Tyley, L. R. 1958 *J. Imp. Chem. Engng. Soc.* **12**, 16.
Swift, H. W. 1952 *J. Mech. Phys. Solids*, **1**, 1.
Weil, N. A. & Newmark, N. M. 1955 *J. Appl. Mech.* **22**, 533.

PHILOSOPHICAL TRANSACTIONS OF THE ROYAL SOCIETY A MATHEMATICAL, PHYSICAL & ENGINEERING SCIENCES

PHILOSOPHICAL TRANSACTIONS OF THE ROYAL SOCIETY A MATHEMATICAL, PHYSICAL & ENGINEERING SCIENCES

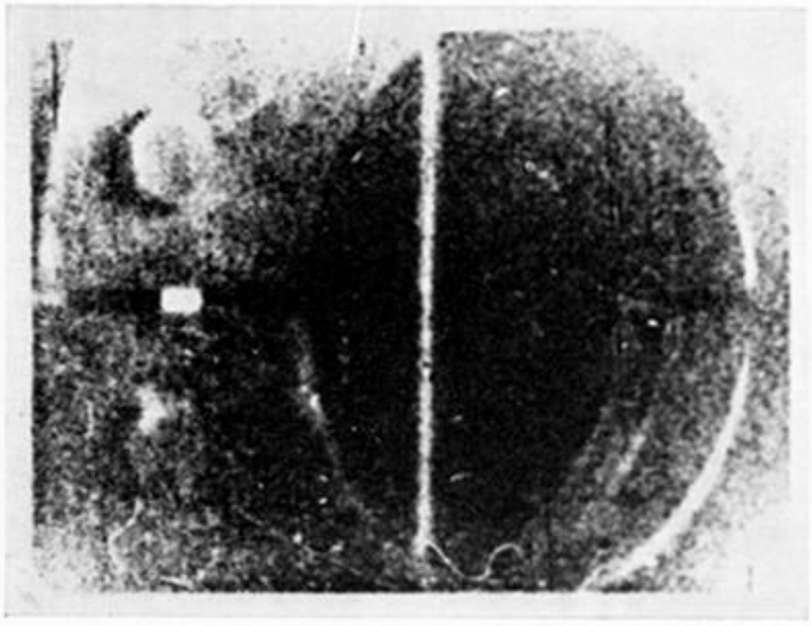

(*a*) $t = 0$

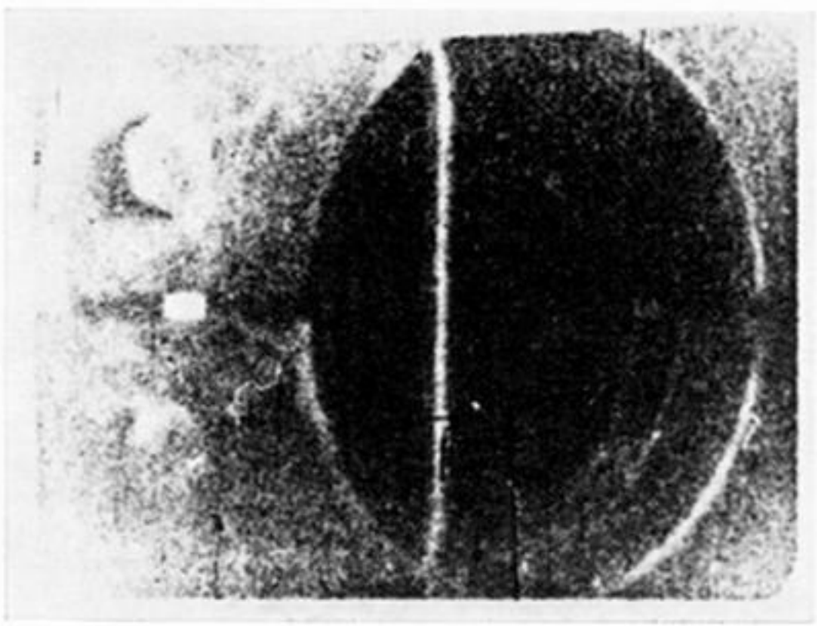

(*b*) $t = 75\ \mu s$

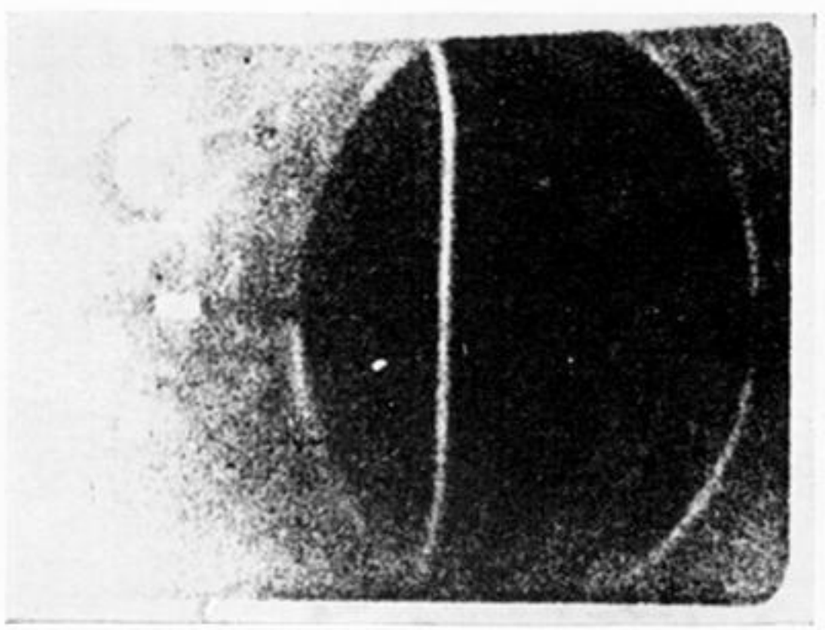

(*c*) $t = 145\ \mu s$

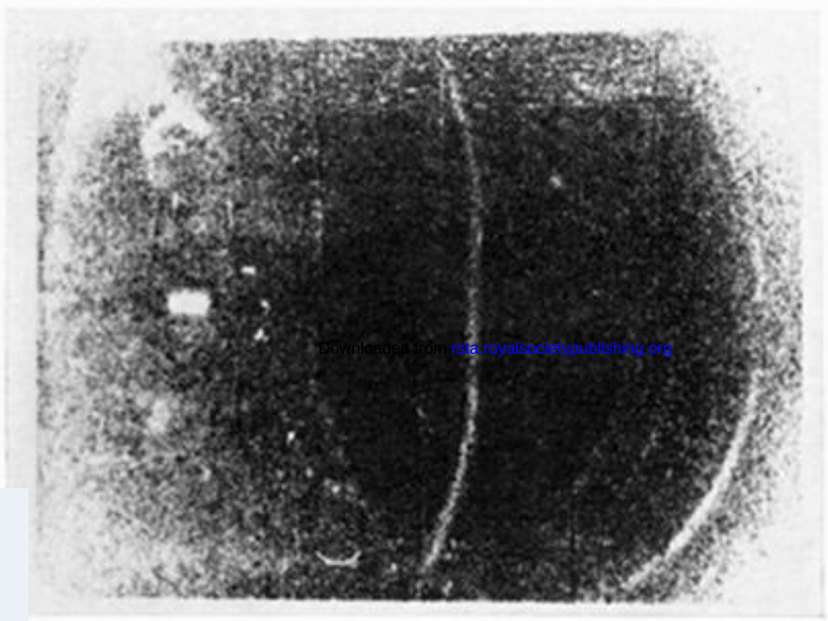

(*d*) $t = 220\ \mu s$

(*e*) $t = 280\ \mu s$

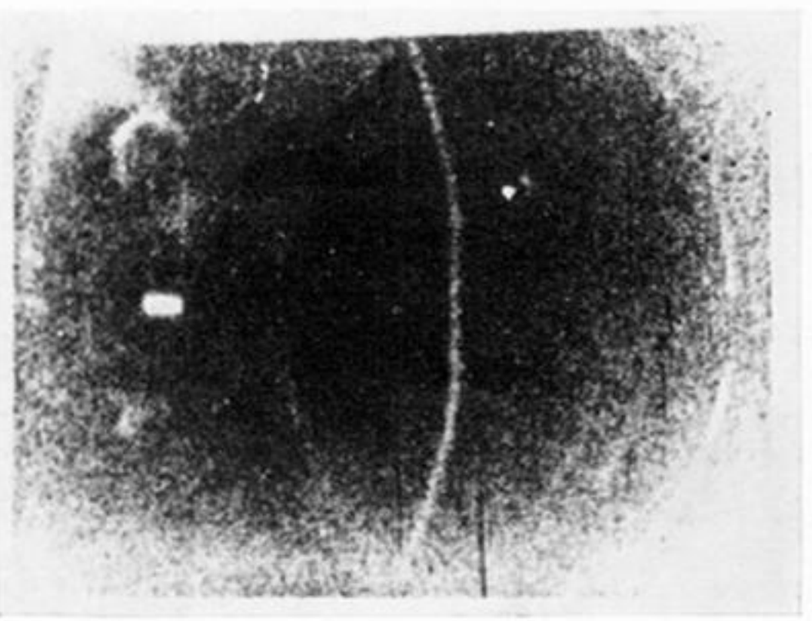

(*f*) $t = 330\ \mu s$

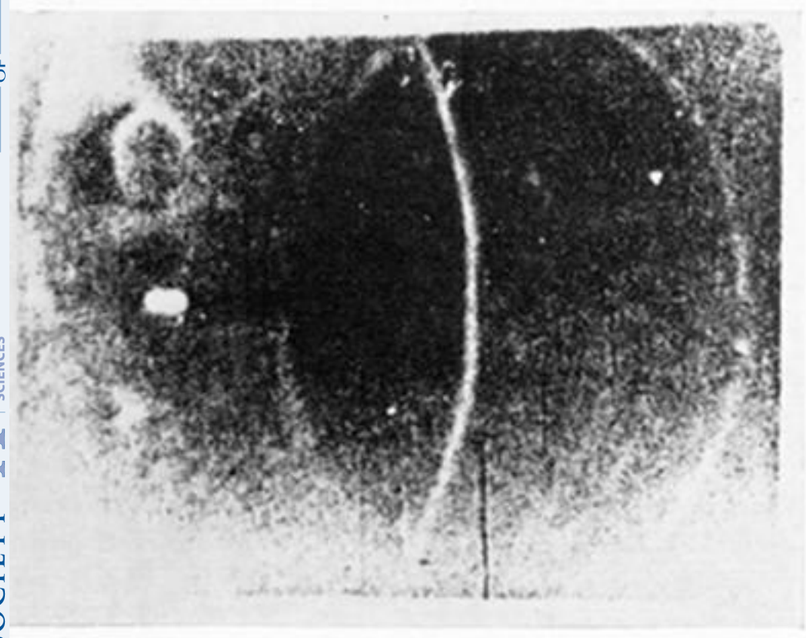

(*g*) $t = 350\ \mu s$

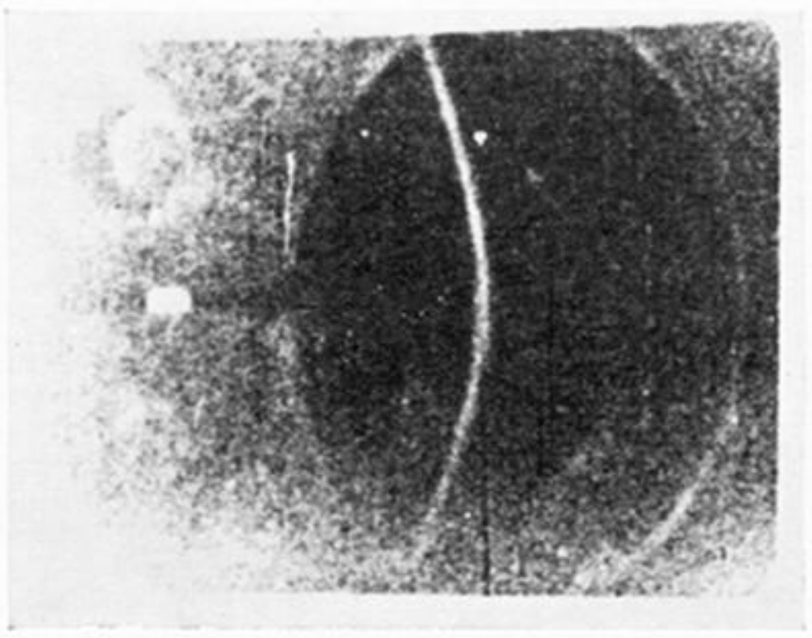

(*h*) $t = 370\ \mu s$

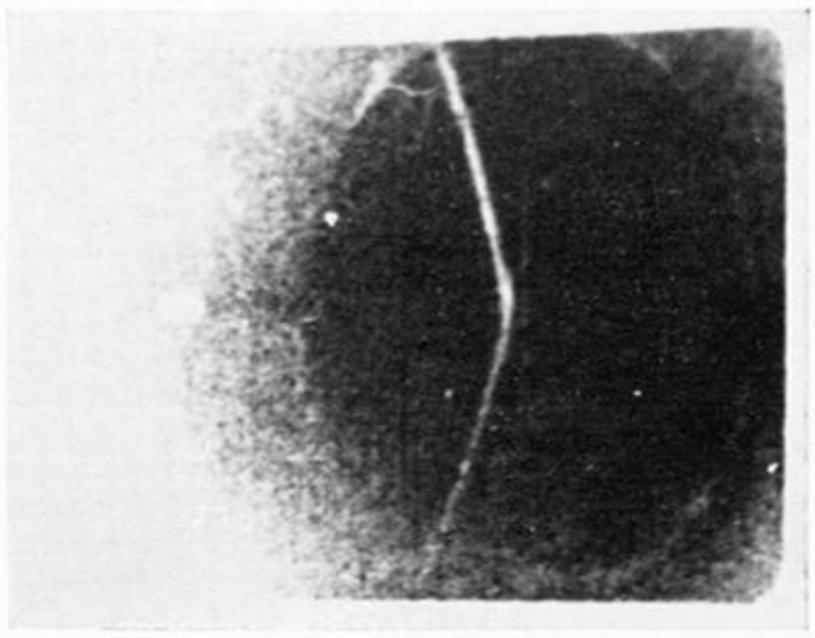

(*i*) $t = 415\ \mu s$

FIGURE 12. High-speed ciné recordings of 6 in. diameter copper disk, 0·0027 in. thick (*ca.* 200 000 pictures per second; approximate time intervals in microseconds).

Downloaded from rsta.royalsocietypublishing.org

PHILOSOPHICAL TRANSACTIONS OF THE ROYAL SOCIETY A MATHEMATICAL, PHYSICAL & ENGINEERING SCIENCES

PHILOSOPHICAL TRANSACTIONS OF THE ROYAL SOCIETY A MATHEMATICAL, PHYSICAL & ENGINEERING SCIENCES

PHILOSOPHICAL TRANSACTIONS OF THE ROYAL SOCIETY A MATHEMATICAL, PHYSICAL & ENGINEERING SCIENCES

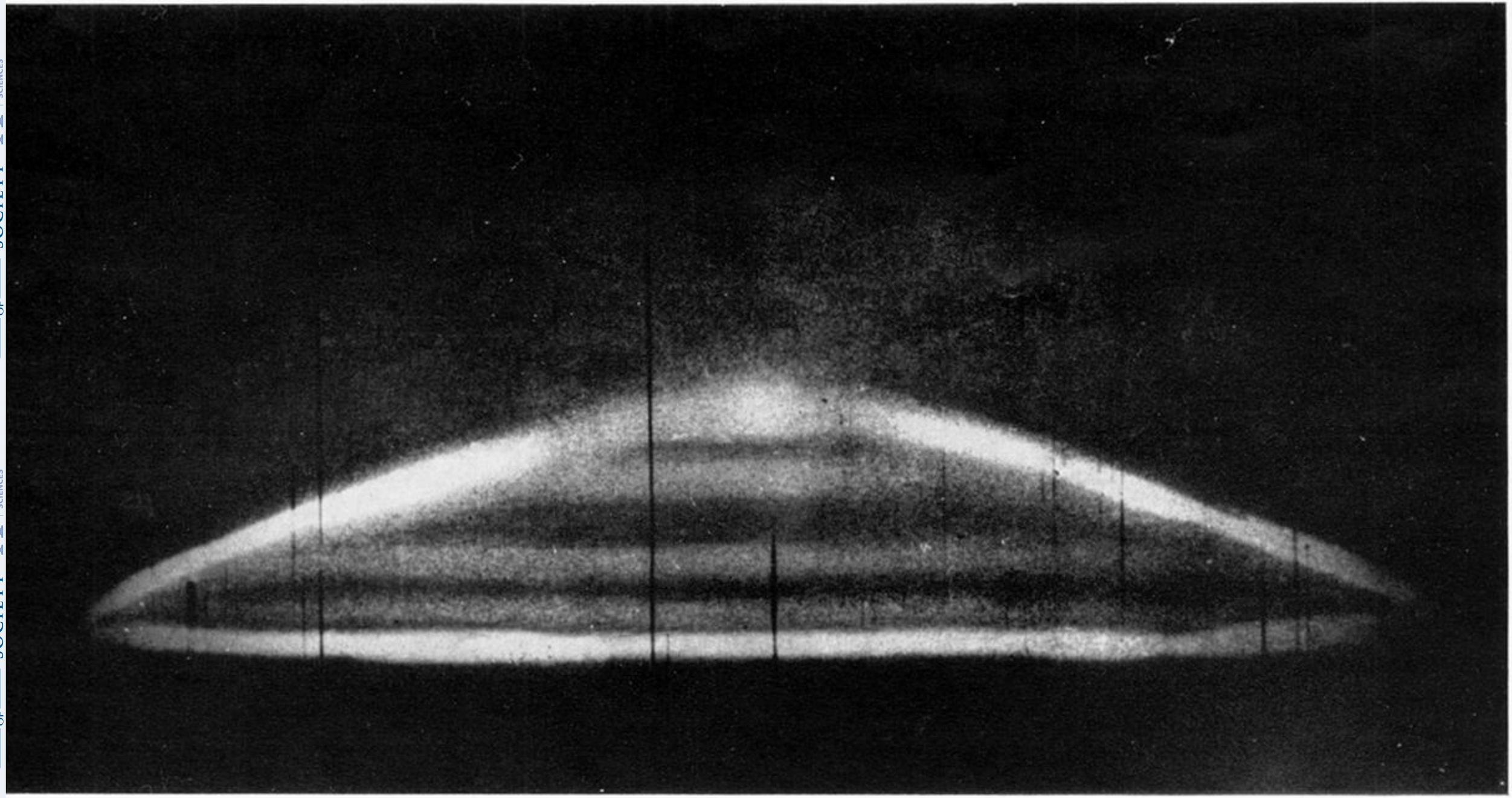

FIGURE 13. Multiple flash photograph of 4 in. diameter copper disk, 0·002 in. thick.

PHILOSOPHICAL TRANSACTIONS OF THE ROYAL SOCIETY A MATHEMATICAL, PHYSICAL & ENGINEERING SCIENCES

Downloaded from rsta.royalsocietypublishing.org

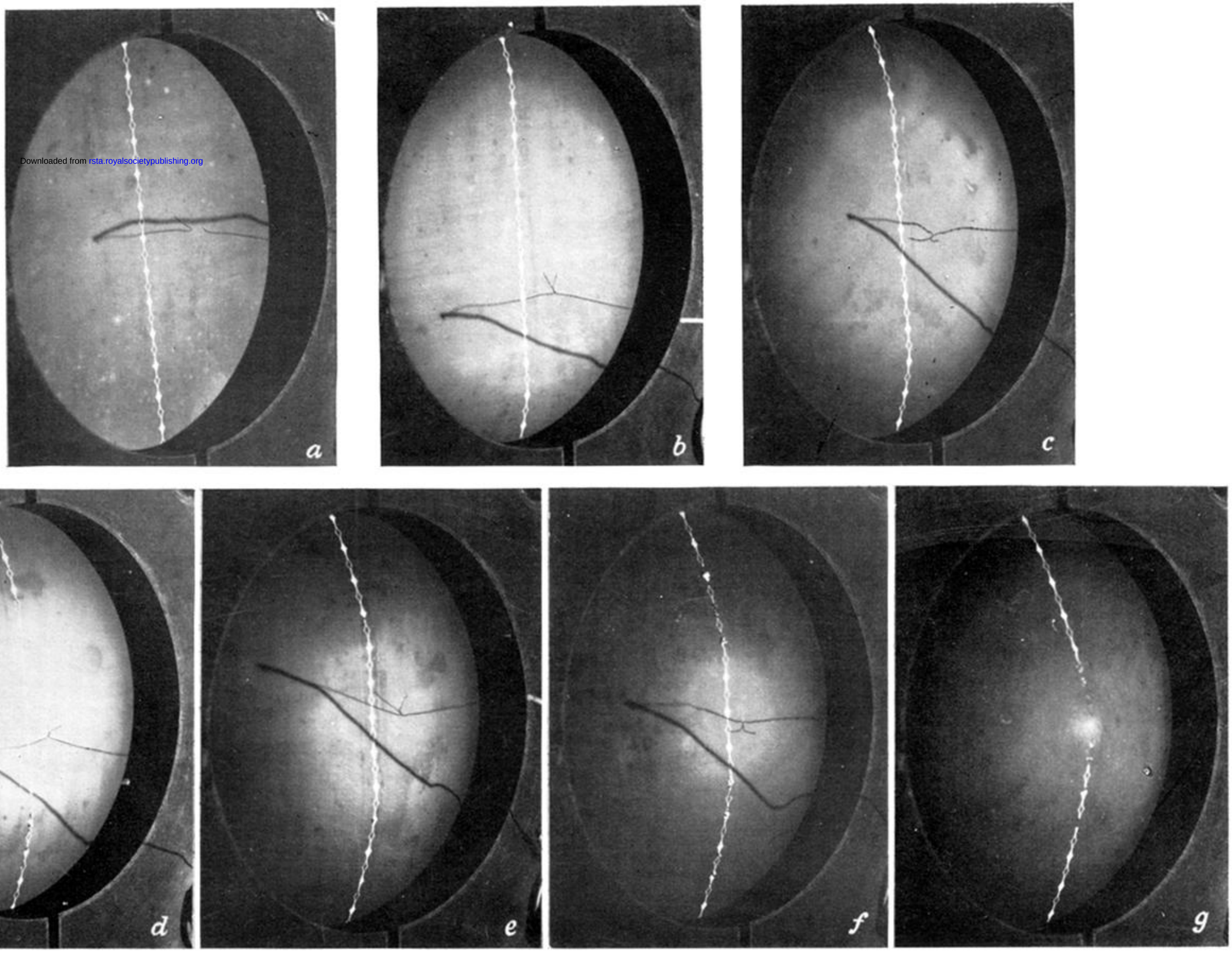

FIGURE 14. Single flash photographs of 6 in. diameter copper disk, 0·002 in. thick.

PHILOSOPHICAL TRANSACTIONS OF THE ROYAL SOCIETY A MATHEMATICAL, PHYSICAL & ENGINEERING SCIENCES

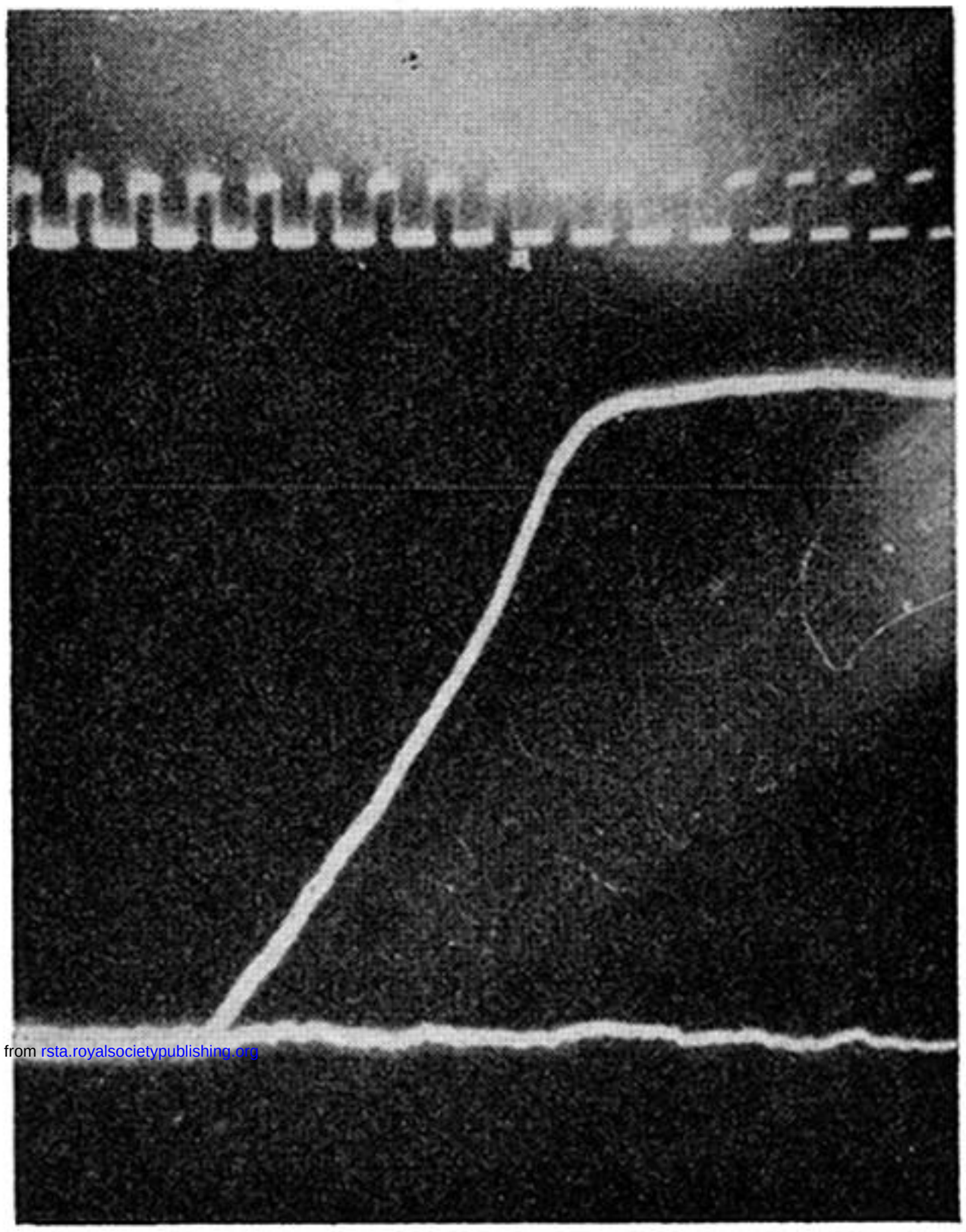

Downloaded from rsta.royalsocietypublishing.org

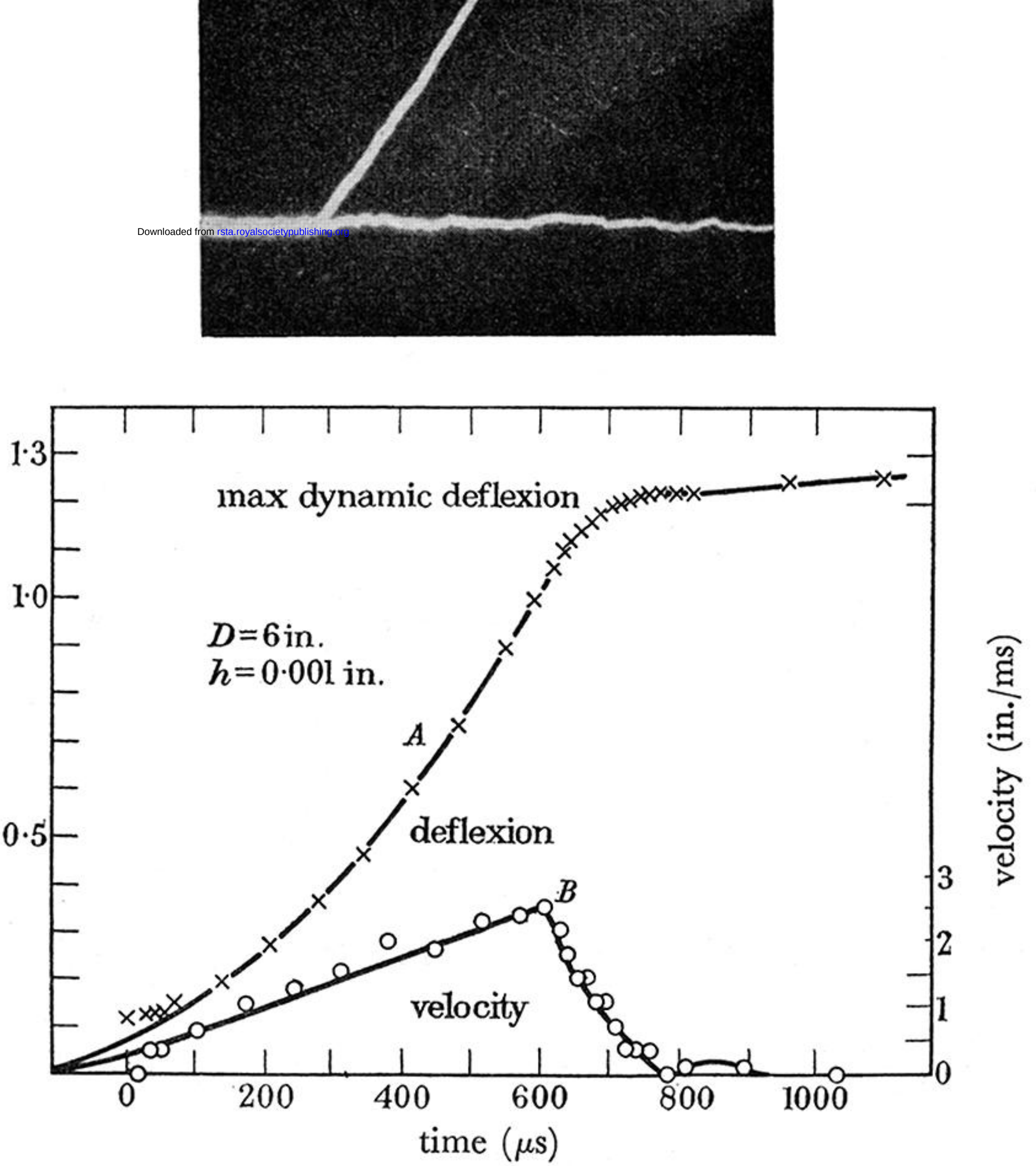

FIGURE 19. Oscilloscope record and measured values.

PHILOSOPHICAL TRANSACTIONS OF THE ROYAL SOCIETY A MATHEMATICAL, PHYSICAL & ENGINEERING SCIENCES